Stony Brook University

Processing and Characterization of ε -WO_3 Processed by Flame Spray Pyrolysis

A Thesis Presented

by

Wen Ling Liao

to

The Graduate School

in Partial Fulfillment of the

Requirements

for the Degree of

Master of Science

in

Materials Science and Engineering

Stony Brook University

December 2014

Stony Brook University

The Graduate School

Wen Ling Liao

We, the thesis committee for the above candidate for the

Master of Science degree, hereby recommend

acceptance of this thesis.

Dr. Pelagia-Irene (Perena) Gouma
Professor, Department of Materials Science and Engineering

Dr. Dilip Gersappe
Professor, Department of Materials Science and Engineering

Dr. Jonathan Sokolov
Professor, Department of Materials Science and Engineering

This thesis is accepted by the Graduate School

Charles Taber
Dean of the Graduate School

Abstract of the Thesis

Processing and Characterization of ε -WO_3 Processed by Flame Spray Pyrolysis

by

Wen Ling Liao

Master of Science

in

Materials Science and Engineering

Stony Brook University

2014

Acetone is one of the biomarkers in our breath that may be used to control metabolic disorders, such as diabetes. Sensors that monitor acetone in breath with high specificity and high sensitivity are needed for this purpose. It has been found previously by our research group that nanostructure ε -phase WO_3 –based sensors are highly selective to acetone compared to other volatile organic compounds found in breath. Since doping in metal oxides usually present stability issues in the long-term operation of a gas sensor, pure ε -WO_3 is being explored as the sensing element of choice for develop a non-invasive method to monitor diabetes based on breath acetone monitoring. However, ε -WO_3 is a thermodynamically unstable polymorph of the WO_3 system at room temperature. Thus rapid solidification processing was employed in this project to synthesize pure ε -WO_3 nanopowders.

This thesis focuses on using flame spray pyrolysis to produce pure ε -WO_3 nanoparticles that can be stable at high temperatures. The flame spray pyrolysis is a scalable

nanomanufacturing process that allows the precursor chemicals (solute) to react with oxygen and the product to nucleate in the reactor when it is far away from the flame source. The advantage of flame spray pyrolysis is that it provides large temperature gradient for the product to nucleate and short residence time for its sintering; therefore, the metastable phase, ε -WO_3, could be synthesized directly from a range of precursors (solutes) in a single step, by increasing the nucleation rate and reducing the residence time.

In this work, isopropanol, xylene and a mixture of them have been used as the precursor solvent materials. Tungsten isopropoxide's raman spectroscopy and XRD analysis showed that the mixing of xylene with tungsten isopropoxide could produce the ε phase at room temperature and that was stable at high temperature following heat treatment. It could be the reason that the xylene has higher evaporative rate than isopropanol so that creating the higher temperature gradient.

In addition, ferroelectric testing on the sample that contains the ε -WO_3 has been conducted. The testing device was served as a parallel-plate capacitor that has gold and copper as top and bottom electrode and the thickness is controlled by the thickness of thin film. The ferroelectric test result does not show the typical butterfly curve on the capacitance. It could be the reason that the film for the device is not thick enough so that a lot of defects to create the current leakage. Another possibility is that the particle size may be too small to observe ferroelectric effects. Suggestions for further studies that build on the current results are also made.

Dedicate to

My parents and my sister

Table of Contents

List of Figures

List of Tables

Acknowledgments

To finish a thesis is not an easy process, thanks for so many people of your support, advice and blessing.

First, I would like to give my great appreciation to my thesis advisor- Prof. Pelagia-Irene (Perena) Gouma. Thanks for introducing this interesting topic regarding the biosensor which I would like work for it during my undergraduate. Also, thanks for giving me the opportunity to work in the BNL for the hands on experience of using the analyzing instruments and meeting with those great scientists. Besides, thanks for giving me the advice and teaching me how to do the research and be a scientist. Lastly, thank you for giving me the opportunity to attend the conference and help me for the poster presentation. Those experiences are really a treasure for me.

Second, I would like to thank Prof. Dilip Gersappe and Prof. Jonathan Sokolov for serving as my thesis committee. Thank you for your kindly agreement. I also would like to give my thankful to all BNL researchers: Fernando Camino, Kim Kisslinger, Tong Xiao, Dmytro Nykypanchuk and Gwen Wright for training me on SEM, TEM, XRD, Raman spectroscopy and ferroelectric testing. In addition, I would like to thank my lab mates Jusang Lee and Gagan Jodhani for the training of FSP and the advice when I hit my bottleneck of my research. Also, my other lab mates Jiahao Huang, Xicheng Jia, Chao Han and Yan Li for all the support. In addition, I would like to thank my friends Eric and Greg for the help on my research and Heidi, Rich, Calvin, Yushek, Mike, Matt for all your support and blessing.

Last but not least, I would like to give my great thankful to my parents, my sister and my family. Thank you all for your kindly consideration and the great support for me. You know how much I love you all.

CHAPTER 1 Introduction

1.1 Tungsten trioxide (WO_3)

Tungsten is a transition metal and its electron configuration is $[Xe]4f^{14}5d^{4}6s^{2}$. With an unfilled outer shell, tungsten exhibits various oxidation states to form numerous oxides such as tungsten (III) oxide, tungsten (IV) oxide and tungsten (VI) oxide. Among all of these oxides, tungsten (VI) oxide, or so-called tungsten trioxide (WO_3), is the most stable one. In this section, the structure of tungsten trioxide and the phase transitions of its bulk state, micro-scale and nano-scale are reviewed.

1.1.1 Structure of tungsten trioxide

The structural unit of tungsten trioxide is the WO_6 octahedron in which six oxygen atoms are at the corner and the tungsten atom is in the center (Tilley, 1995). Each WO_6 octahedron shares corner oxygen atoms with others to form the three dimensional network creating the basic structure of tungsten trioxide as displayed in Figure 1-1. This three dimensional network creates a perfect cube, as same as the ReO_3 cubic structure, but it can only be seen in the idealized structure of WO_3. Under real conditions, the tungsten atom displaces from the center of an octahedron because the size of tungsten atom is small, thus distorting the cubic structure (Tilley, 1995). The amount of the displacement for the tungsten atom depends on the temperature. Therefore, different crystalline structures can be seen under different temperatures to cause the phase transition of tungsten trioxide.

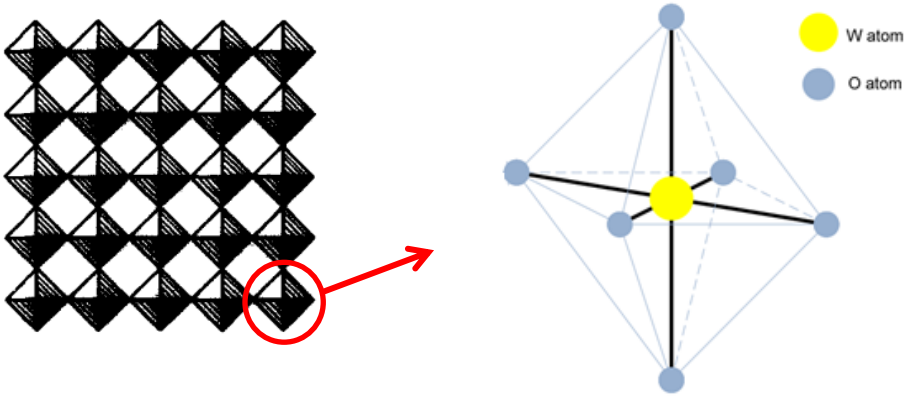

Figure 1-1 Basic structure of WO_3 and the unit cell of WO_6 octahedron. (Edited from (Tilley, 1995) and (Lisheng Wang's dissertation) respectively)

1.1.2 Phases transition of bulk tungsten trioxide

Tungsten trioxide undergoes phase transformations with increasing temperature as it was concluded from the observed discontinuities of its thermal and electrical properties. Based on the Sawada (1956) and Foex (1945and 1949) studies, the structure changes at -50, -20, 330, 740, 910 and 1230 ℃ manifested in the abrupt changes in the electrical resistivity and specific heat (Salje & Viswanathan, 1975). The crystallographic symmetry of WO_3 was refined by Taniskai in 1960 by conducting X-ray analysis. From those early studies the crystal structure of bulk WO_3 crystals was deduced from -70 ℃ to 1250 ℃ with the increasing of temperature to be in the sequence of: monoclinic, triclinic, monoclinic, orthorhombic and tetragonal (Tanisaki, 1960a, 1960b). This sequence has been supplemented with information on space groups and lattice parameters for each polymorphic structure. Nowadays, the sequence of polymorphic phase transitions of bulk tungsten trioxide (i.e. the dimension of the grain configuration is in mm scale) between

absolute zero and its melting point (around 1427 ℃) has been well studied as summarized in Table 1. Each phase structure is shown in Figure 1-2.

Table 1 Summary of bulk tungsten trioxide phase transitions (Malin et al., 2013)

Structure	Space group	Symbol	Temperature
monoclinic	Pc	ε -WO_3	-273 ℃ ~ -43 ℃
triclinic	$P\bar{1}$	δ -WO_3	-43 ℃ ~ 27 ℃
monoclinic	$P2_1/n$	γ - WO3	27 ℃ ~ 350 ℃
orthorhombic	Pmnb	β - WO_3	350 ℃ ~ 680 ℃
tetragonal	P_4/ncc	α - WO_3	680 ℃ ~ 898 ℃
tetragonal	P_4/nmm	α - WO_3	898 ℃ ~ 1427 ℃

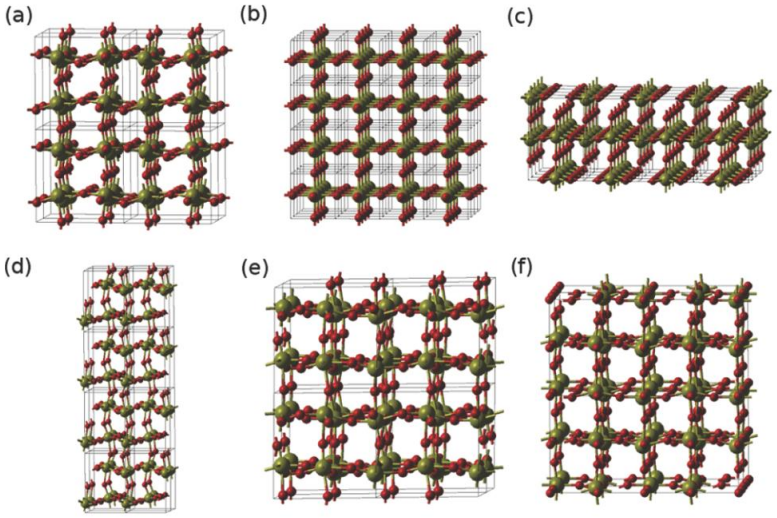

Figure 1-2 The structure of (a) γ - WO_3 (b) cubic (c) α - WO_3 (d) ε -WO_3 (e) δ -WO_3 (f) β - WO_3 (F. Wang, Di Valentin, & Pacchioni, 2011)

There are two factors that affect the phase transition for tungsten trioxide: distortion and tilting of WO_6 octahedra. The distortion of WO_6 octahedra is due to the displacement of the tungsten atom as described in section 1.1.1. The tilting of WO_6 octahedra means the c-axis or a-axis is rotating or tilting an angle away from the cubic structure as shown in Figure 1-3(Ekhard et al., 1997). Either one or both of these factors can been seen to give rise to a phase transition.

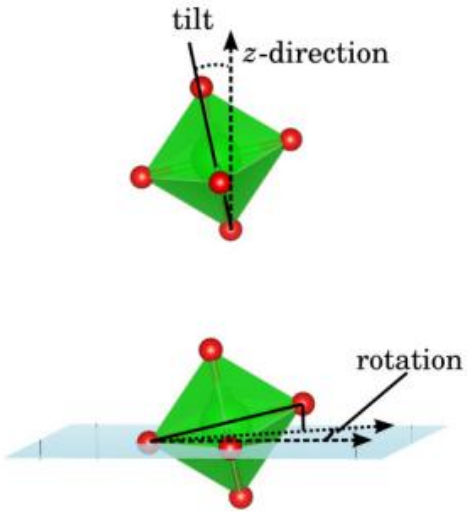

Figure 1-3 The scheme illustrates the tilting of WO_6 octahedra (Schick, Jiang, Saldana-Greco, & Rappe, 2014)

However, when the dimension of tungsten trioxide goes down to micro- or nanoscales, the phase transformation does not undergo the same sequence as shown in Table 1 which will be further discuss in Section 1.1.3.

1.1.3 Phase transition of micro and nano scale tungsten trioxide

When the crystal size of the tungsten trioxide goes down to micro or nano scale, the phase that presented at or below room temperature would not follow the trends that bulk tungsten trioxide showed in Table 1. Still, the high temperature phase (orthorhombic and tetragonal phase) remains the same regardless of the crystal size of the material (Cazzanelli, Vinegoni, Mariotto, Kuzmin, & Purans, 1999). However, the tungsten trioxide micro and nanocrystal undergo phase transitions at low temperature that depended on the synthesis method used to fabricate the oxide (Arai, Hayashi, Yamamoto, & Kim, 1990; Cazzanelli, Vinegoni, et al., 1999; Filho et al., 2001). In addition, polymorphic phase change may be achieved by mechanical treatment (Cazzanelli, Mariotto, Vinegoni, Kuzmin, & Purans, 1999; Cazzanelli, Vinegoni, et al., 1999; Kuzmin, Purans, Cazzanelli, Vinegoni, & Mariotto, 1998) or by varying the pressure condition at the same temperature. The factors that affect the phase transitions in micro-/nano-scale are discussed in the following sections:

- Synthesis method

The gas evaporation method synthesized tungsten trioxide microcrystal in the range of 100 nm to 180 nm under the mixture of Ar and O_2 atmosphere has been found the phase transition as Table 2 shown. In this studied, they found a new phase under the room temperature and gradual phase transition when temperature approaches the room temperature (Arai et al., 1990). They also found that the crystal size decreased with the decreasing temperature; therefore, they concluded that the changing of the crystal size is the reason for causing phase transition. Their conclusion has been proven by Hayashi et

al.'s study. It showed that the larger crystals tend to present γ – phase at room temperature and a new phase below the room temperature. The smaller crystals tend to be ε - phase at both room temperature and below room temperature (Hayashi, Sugano, Arai, & Yamamoto, 1992).

Table 2 Summary of phase transition for gas-evaporated WO_3 microcrystals (Arai et al., 1990)

Phase	Temperature
New phase + ε – phase or New phase only	-263 ℃ ~ -73 ℃
Gradual transition	-73 ℃ ~ -13 ℃
γ – phase + ε – phase	-13 ℃ ~ 327 ℃
Orthorhombic	327 ℃ ~ 737 ℃
tetragonal	737 ℃ ~ 1427 ℃

The phase transition of commercial 99.998 % WO_3 powder which used for optical industry and had the crystal size in the micron scale is shown in Table 3. When compared their phase transition to bulk tungsten trioxide, the typical low temperature phases, ε – phase and δ – phase did not be detected; instead, they found the new phase which shown in gas-evaporated WO_3 dominated below 120 K and eventually vanished at 200 K by transforming into γ – phase (Cazzanelli, Vinegoni, et al., 1999). The reason that ε – phase was absent is because of the larger crystal size for the powder compared with the gas-evaporated WO_3. This proved that larger crystals tend to be in γ – phase at room temperature and transformed to new phase when the temperature decreased (Cazzanelli, Mariotto, et al., 1999; Cazzanelli, Vinegoni, et al., 1999).

Table 3 Summary of phase transition for pure WO_3 powder (Cazzanelli, Vinegoni, et al., 1999)

Phase	Temperature
New phase + γ – phase	-233 ℃ ~ -53 ℃
Gradual transition	-133 ℃ ~ -33 ℃
γ – phase	-13 ℃ ~ 327 ℃
Orthorhombic	327 ℃ ~ 737 ℃
Tetragonal	737 ℃ ~ 1427 ℃

WO_3 microcrystals by thermal decomposition of ammonium paratungstate was studied the phase transition after 973 K sintering for more than an hour (Filho et al., 2001). The crystal size of the sintered WO_3 is 210 nm and the phase transition of it is summarized in Table 4. Before sintering process, the phase that existed at room temperature is γ – phase but it changed to phase separation of γ – phase and δ – phase. It is remarkable that different sintering temperatures showed the same result that γ – phase and δ – phase co-existed at room temperature. The only difference between the various sintering temperatures was the different ratio of γ – phase and δ – phase (Souza-Filho et al., 2000) .

In summary, the synthesis method affects the phase transition of microcrystals at low temperature is relating to the grain size. Because the grain size strongly influenced by the synthesizing method and temperature, it is hard to predict the trends of the phase transition for micro and nano scale tungsten trioxide.

Table 4 Summary of phase transition for WO_3 powder undergo sintering process (Filho et al., 2001)

Phase	Temperature
ε – phase + new phase	-243 ℃
Gradual transition	-133 ℃ ~ -33 ℃
δ – phase + γ – phase	-33 ℃ ~ 27 ℃
Orthorhombic	327 ℃ ~ 737 ℃
Tetragonal	737 ℃ ~ 1427 ℃

- Mechanical treatment

Other than the temperature, the mechanical treatment will also affect the phase transition for microcrystalline tungsten trioxides. It has been found that the grinding process would affect the grain size so that it influences the phase transition. At the initial grinding stage, the grain size dramatically decreased and eventually reduction rate slows down (Kuzmin et al., 1998). Further studies involved mild and strong mechanical treatment. The mild treatment is conducted by compressing the WO_3 powder for few minutes. On the other hand, the strong mechanical treatment is done by ball milling machine for an hour (Cazzanelli, Vinegoni, et al., 1999).

For the mild milling treatment, the phase changed gradually from γ – phase to δ – phase at room temperature which showed the same phase trend as the fast cooling process of virgin sample. In addition, the changed phase could last long unless annealing it with higher temperature. However, when we applied cooling process on the mild-

treated sample, a weak phase transition from δ – phase to new phase has been observed. In other words, the δ – phase still dominated in the mild-treated sample even when the temperature decreased. On the other hand, under strong mechanical treatment condition, a small portion of grains would undergo the phase transition from δ – phase to ε – phase at room temperature (Cazzanelli, Vinegoni, et al., 1999).

- Pressure

At the beginning of the pressure studied, the phase was found to change from γ – phase to δ – phase and promoted to ε – phase with further pressure input at room temperature (Cazzanelli, Vinegoni, et al., 1999). On the contrary, when applying pressure on bulk tungsten trioxide to 47 kbar, a stable high pressure phase has been found: monoclinic space group symmetry $P2_1/c$. It has been shown that the phase transformed reversibly between 0.3 and 1.2 kbar (Xu, Carlson, & Norrestam, 1997). Different from the bulk material, the microcrystal WO_3 would partially retain the high pressure phase ($P2_1/c$) even pressure released. A studied of applying high pressure to 4 GPa on the microcrystal WO_3 found that the phase would gradually change to high pressure phase from the original coexistence of γ – phase and δ – phase (Souza Filho et al., 2000). The same perspective between the bulk and the micro-WO_3 is that the phase changed to space group of $P2_1/c$ at lower pressure and remained at the same phase even in higher pressure.

1.2 Epsilon Phase (ε-WO_3)

1.2.1 Structure of ε-WO_3

The structure of ε – phase is monoclinic with the lattice parameter of a = 5.278 Å, b = 5.156 Å, c = 7.664 Å, and β = 91.762˚ which belongs to the space group of Pc (Woodward, Sleight, & Vogt, 1997). The structure of ε – phase is shown in Figure 1-4 and the comparison with other common low temperature phases, γ – phase and δ – phase, is presented in Figure 1-5. It is interesting to see that the phase transition of δ – phase to ε – phase is because of the distortion of WO_6 octahedra only; in other words, the position of tungsten atom has been shifted. Generally, the driving force of phase transition for tungsten trioxide is related to both the distortion and the tilting of WO_6 octahedra as described in section 1.1.2 (Woodward et al., 1997). In addition, it has been found that the structure of tungsten trioxide from high temperature to room temperature lowered the symmetry but the phase transited from δ – phase to ε – phase increased the symmetry (triclinic to monoclinic). The reason for the increasing of symmetry is because only distortion of WO_6 octahedra took place to drive the phase transition process of δ – phase to ε – phase (Woodward et al., 1997).

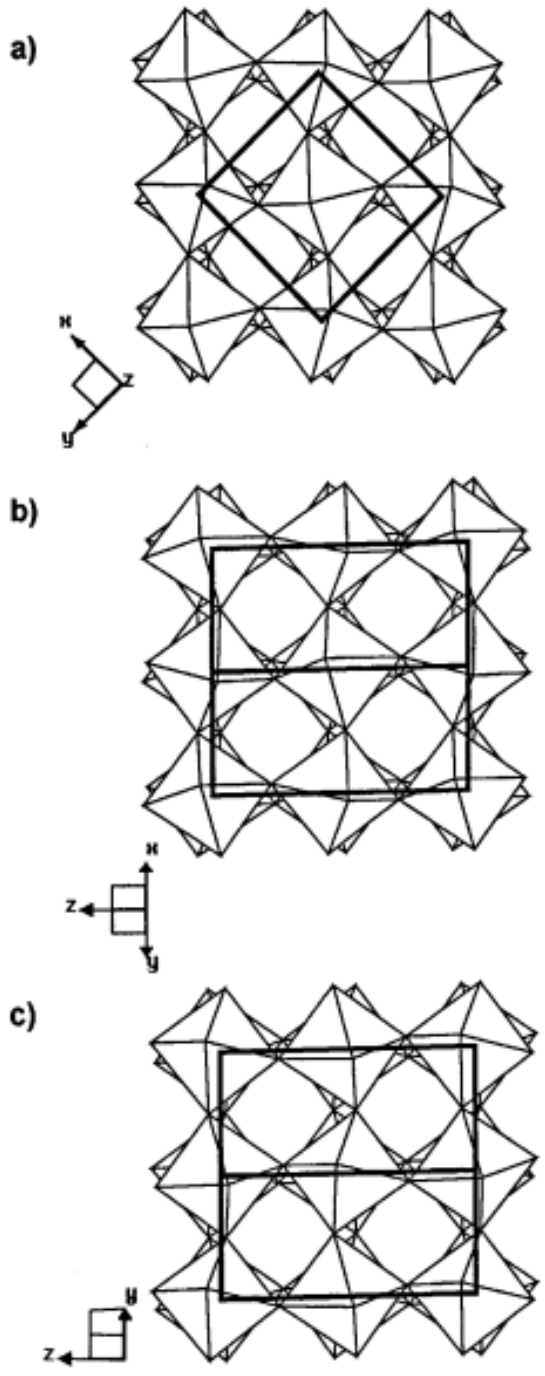

Figure 1-4 Structure of ε-WO_3 looking down from the direction of (a) [001] (b) [$\bar{1}\bar{1}0$] (c) [110]. (Woodward et al., 1997)

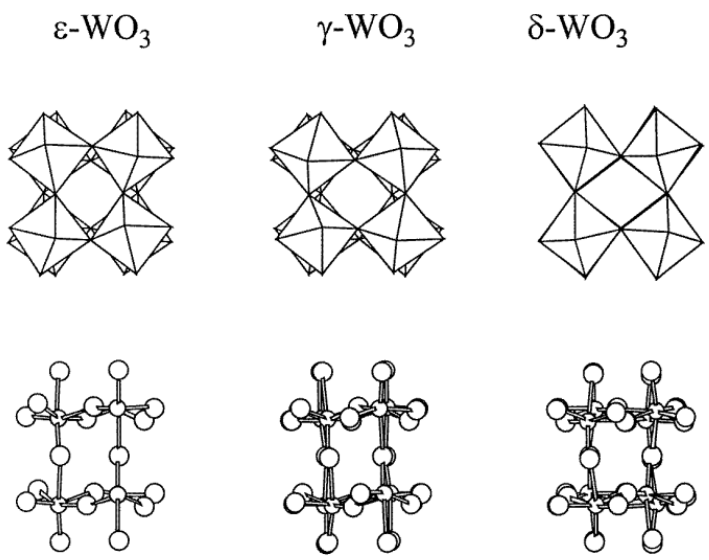

Figure 1-5 The structure comparison between low temperature phases (Ekhard et al., 1997)

Compared with the other five phases of tungsten trioxide, ε – phase has unique physical properties such as it is ferroelectric (Sawada, 1956), exhibits anisotropic electrical transport (Woodward et al., 1997), and has an electric dipole moment (Ekhard et al., 1997). Those unique physical properties are derived from its structure. It has been found that the tungsten atoms shifted in the z direction is not equal at the positive and negative direction in the ε – phase; therefore, the net spontaneous polarization would be developed along the c-axis of the unit cell of WO_3. Similarly, the tungsten atoms shifted in x direction is not comparable to the shift in y direction, causing the net spontaneous polarization be developed along the a-axis of the unit cell. The combination of the two axis spontaneous polarization results in the observation of hysteresis loop of ferroelectric in the ε – phase (Woodward et al., 1997). Besides, the tungsten atoms displace unequally

in different direction causing the volume contraction and band gap changing as well. The unique physical properties of ε – phase would be discussed in detail in section 1.2.2.

1.2.2 Physical properties of ε-WO_3

The evidence of phase transition from δ – phase to ε – phase is the sudden changing of physical properties. It has been found that the electrical resistivity increased 10 to 30 fold (Salje & Viswanathan, 1975; Tanisaki, 1960b), the optical band gap increased causing the color changed to bluish white (Salje & Viswanathan, 1975), volume contracted (Woodward et al., 1997) and ferroelectric behavior presented (Salje & Viswanathan, 1975) during the phase transition.

The optical properties of ε – phase has been studied via the absorption spectrum so as to investigate the band gap and the color changed. The color of WO_3 was brownish yellow at room temperature. It changed to pale green and eventually to bluish white, the color that ε – phase shown, when lowered the temperature. Besides, at the transition temperature of ε – phase, the absorption spectrum showed the typical semiconductors' absorption edge indicating the ε – phase is semiconducting which showed the same result as the electrical resistivity testing (Salje & Viswanathan, 1975). If the electrical resistivity increased with the increasing temperature, the material is metallic. On the other hand, the semiconducting material would show the decreasing of resistivity with the increasing temperature. Since the electrical resistivity increased during the phase transition from δ – phase to ε – phase, both of these phases were semiconducting (Hirose, 1980).

The most unique physical properties for ε – phase is ferroelectric. The ferroelectric property was discovered because high permittivity was observed (Sawada,

1956). Following the discovery of the hysteresis phenomenon, the independently ferroelectric properties of tungsten trioxide has been reported (Matthias, 1949). Finally, Hirakawa observed a hysteresis loop below the room temperature and it disappeared during the heating process. This result pointed out the ferroelectric properties ε – phase own (Sawada, 1956). The reason that ε – phase is ferroelectric is because of its structure which, as described in section 1.2.1, creates a non-vanishing electric dipole at z direction.

1.2.3 ε – phase presents at room temperature

From the phase transition of bulk tungsten trioxide, the common phases that we could observe at room temperature are δ – phase and γ – phase. Usually the ε – phase could only be observed below the room temperature. However, there are some studies showed that ε – phase present at room temperature. For example, gas evaporated WO_3 microcrystals and commercial powder after strong mechanical treatment were described in section 1.1.3 both showed the observation of ε – phase at room temperature.

Other than these two studies above, some other methods to synthesize the tungsten trioxide also produced the ε – phase at room temperature. The tungsten trioxide thin film synthesized by reactive DC magnetron sputtering of pure tungsten under the atmosphere of oxygen and argon in the ratio of 0.43 has also given the ε – phase. In those studies, the phase for the as-received tungsten trioxide thin film observed was the stable room temperature phase: γ – phase. However, when higher pressure was applied to the sample, some γ – phase transformed to the ε – phase and has phase separation in the sample. They found that when applied the pressure at 20 and 25 mTorr, the coexistence

of γ – phase and ε – phase can be detected but when operated at 30 mTorr, the ε – phase was not obvious enough (Malin et al., 2013).

In addition, the flame spray pyrolysis synthesis of tungsten trioxide nanoparticles from a mixture of ammonium tungstate hydrate with diethylene glycol monbutyl ether and ethanol showed the coexistence of γ – phase and ε – phase in the as-received powders at room temperature. These authors (Lisheng Wang's dissertation) also found that the grain size would affect the percentage of the ε – phase presented in the sample. Based on those studies, the smallest particle would have around 72.4 % of ε – phase preserved at room temperature while the largest particle had approximately 31.3 %. However, after the heat treatment at 500 ℃ for 8 hours, some of the ε – phase transformed to γ – phase because the heating process enlarged the grain size. These authors showed that the smallest grain size had 31.6 % ε – phase left and the largest one had only 2.2 % left (Lisheng Wang's dissertation).

Furthermore, doping the tungsten trioxide with another element was shown to stabilize the ε – phase at room temperature or even after heat treatment. The WO_3 synthesized with flame spray pyrolysis have been studied for doping Cr and Mn. In the case of doping Cr indicated that the higher at % of Cr doped in the WO_3, the more ε – phase could be detected. In addition, the sample that doping with Cr no matter how much at % of Cr has been doped in the tungsten trioxide, the ε – phase would not undergo phase transition after heat treatment. Moreover, the more at % of Cr, the more stable the ε – phase would be during the heating process. On the other hand, the doping with Mn did not show the same effect as the doping of Cr. For the as-synthesized particle, the percentage of ε – phase is in the range of 80.4 % and 69.3 % which presented higher

content of ε – phase than pure tungsten trioxide. Nevertheless, the Mn-doped WO_3 could not maintain the ε – phase content after heat treatment. There was only 32.2 % to 55 % ε – phase left. Comparing to the heat-treated pure tungsten trioxide, it was still a large amount of the ε – phase remained in the samples (Lisheng Wang's dissertation). Further studies for the above flame spray pyrolysis synthesized tungsten trioxide nanoparticles involved doping with Si. 10 % doping of Si could get 100 % ε – phase for the as-synthesized sample and 87 % left after the heat treatment (Marco & Antonio, 2011).

Lastly, the doping of Nb in tungsten trioxide also showed the present of ε – phase at room temperature. The tungsten trioxide thin film that made by pulsed spray pyrolysis deposition technique has been doped with Nb by adding niobium tartarate in the precursor. The result showed that no matter how much percentage of Nb has been added into the tungsten trioxide thin film, the ε – phase would always exist and the grain size of WO_3 was in the range of 20 nm to 60 nm. For comparison, pure tungsten trioxide thin films showed the γ – phase in the sample. However, the authors did not disclose how the amount of ε – phase varied with the percentage of Nb added into the thin film (Suvarna & Patil, 2007).

In conclusion, earlier studies showed that the higher the doping level of the tungsten trioxide the higher the volume fraction of the ε – phase, based on the flame spray pyrolysis method. The mechanism of ε – phase presented in the pure tungsten trioxide at room temperature proposed was that ε – phase was stabilized due to the rapid cooling involved in the flame spray pyrolysis process (Lisheng Wang's dissertation).

1.3 Processing of ε – phase WO_3

ε – phase was preserved at room temperature as a result of a small particle size obtained by rapid solidification processing. The synthesis methods reported for producing ε – phase in pure or doped WO_3 were either gas evaporation, ball milling mechanical treatment, reactive DC magnetron sputtering, pulsed spray pyrolysis or flame spray pyrolysis. Those processing methods are commonly used to produce nanopowders and thin films. These synthesis methods are detailed below and the comparison is shown in Table 5.

Table 5 Comparison between the processing methods for synthesizing ε – phase

Processing	Advantage	Disadvantage	Reference
Gas evaporation	Simple and cheap	The temperature for different material to evaporate is different	
Ball milling	Simple and cheap, applicable to all classes of materials	Contamination	(Kaito, Kimura, & Saito, 1999)
Reactive magnetron sputtering	Capable of producing controllable composition thin film, high deposition rate, wide range for applied power	Arc event	(Safi, 2000)
Spray pyrolysis	Easy to dope, no high quality targets needed, no high vacuum required, easily controlled the deposition rate, processing temperature is moderate, the composition is easily controlled	External flame or power is needed	(Patil, 1999)
Flame spray pyrolysis	Provide self-sustaining and high temperature flame, the usage of less volatile precursors, create large temperature gradients		(Teoh, Amal, & Madler, 2010)

1.3.1 Gas evaporation

The basic concept for gas evaporation to produce micro or nanoscale particles is heating up the material into the vapor state with an evaporation source. The vapor would cool down rapidly and condense into multiple particles. The schematic illustration for the processing of gas evaporation can be seen in Figure 1-6.

During the evaporation process, the atmosphere would be full of inert gas, usually Ar, which would collide with the vapor forming clusters. Usually, the vapor forms a few mm away from the evaporation source so that the clusters could only be detected within this range. Each cluster can still collide with others to form ultrafine particles. This process called coalescence. Since the particle could be visible as smoke during the experiment, they are also named smoke particles. As a result, the size of particles would increase with the distance far from the evaporation source. The growing rate for the particles can be calculated from the following formula:

$$\frac{dr}{dt} = \frac{mk}{4\pi\rho}$$

r: particle radius

m: mass density = total mass of particles per smoke volume

k: coalescence probability factor

From the formula given above, it is noticeable that the particle size is controlled by the mass density and the coalescence probability factor which is dependent on the temperature of the smoke and gas pressure (Kaito et al., 1999). The temperature of smoke

is controlled by the evaporation temperature. Since each material has their coalescence temperature, the distance where the clusters start to coalescence would be strongly affected by the temperature profile of the smoke (Kaito et al., 1999).

On the other hand, those free space particles would be transported with the aid of two flows: the convection flow and the stationary gas flow. The convection flow was original from the evaporation source and the stationary gas flow was observed from the as-synthesized particles. Typically, the spherical particles is formed near the evaporation source and changed to octahedron, cubic or other structure during the transportation. The latest structure is dependent on their crystal structure. (Kaito et al., 1999).

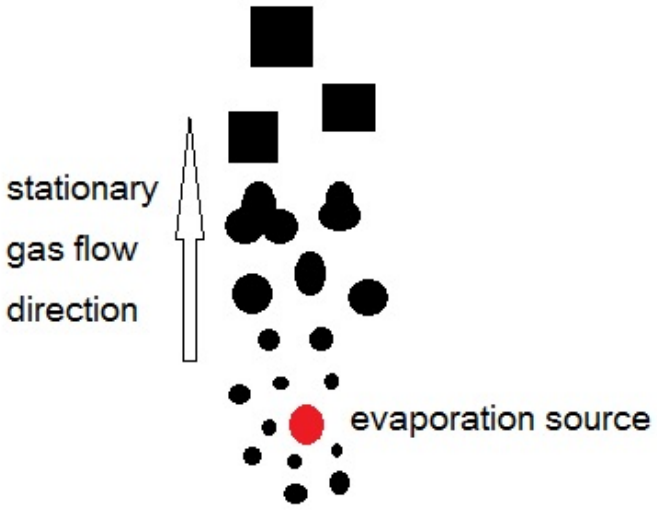

Figure 1-6 The illustration of particle formation in gas evaporation process (Kaito et al., 1999)

1.3.2 Ball milling

Ball milling, or so-called mechanical attrition is the process to introduce the mechanical force on powders so that they would undergo the plastic deformation to decompose the grain into multiply nanoparticles. The concept for this synthesis method is different from other methods which produce the nanoparticles by assembling clusters. The particle size depends on the milling time and the milling temperature. It has been found that the longer milling time and the lower milling temperature can give smaller grain sizes (Koch, 1997).

The mechanism for ball milling is to lower the grain size due to dislocation movement. At the initial stage of the deformation, numerous dislocations would be produced in localized shear bands. Those dislocations would move and eventually annihilate and recombine to form the grain boundary and separate one particle into two individual grains. The last stage was the recovery of the grain by heat treatment. Therefore, the grain size is the competition between plastic deformations caused by dislocations and the structure recovery from the thermal treatment (Koch, 1997).

1.3.3 Reactive magnetron sputtering

Reactive magnetron sputtering is one of the techniques for sputtering process, a type of physical vapor deposition technique. The concept for sputtering is using energetic ions that produced from the discharge plasma to bombard the target and remove the atoms from it. The removal atoms would condense and form a thin film on the substrate. Other than the target atoms, secondary electrons also produced during the bombardment and used to maintain the plasma. But the basic sputtering process has the drawback of

low thin film deposition rates and low ionization efficiencies so that the film was not dense (Sigmund, 1981). The way to solve this problem is magnetron sputtering. A magnetic field is applied parallel to the target surface so that the secondary electrons can be constrained near the target so as to increase the efficiencies of ionization and the deposition rate and allow operating in lower voltage and pressure condition (Kelly & Arnell, 2000).

On the other hand, the reactive sputtering is another sputtering technique that injected the chemically reactive gases so that they will react with the target surface (Musil & Kadlec, 1990). With this method we could form the thin film different from the target material. Usually this technique would be combined with the magnetron sputtering so that it could control the composition of the thin film at higher deposition rates. Therefore, the reactive magnetron sputtering usually formed the dense and defect-free oxide thin film under a controllable oxygen atmosphere (Safi, 2000). The energy source for the reactive magnetron sputtering technique did not restrict to the radio frequency systems because the target is conductive metal so that the direct current (DC) could be used as well. Besides, the metallic target is not only electrically conductive but also thermally conductive; the cooling of the target would be quicker so that the range for applying the power is large. However, this technique has the drawback of the arc events. The arc event is because the insulating layer formed on the target due to the usage of DC power. When bombarding the target, both the insulating layer and the metallic layer would be bombarded. The combination of both two layers bombarded particles was like a capacitor in the viewpoint of electron that creating an internal electric field. Since the

direction of the internal electric field has opposite direction as the external electric field, the action of bombardment would stop eventually (Safi, 2000).

Since particles produced by this process are formed at the substrate, the crystal size was controlled by the substrate temperature. The higher substrate temperature gave us larger grain size and vice versa (Zheng et al., 2011).

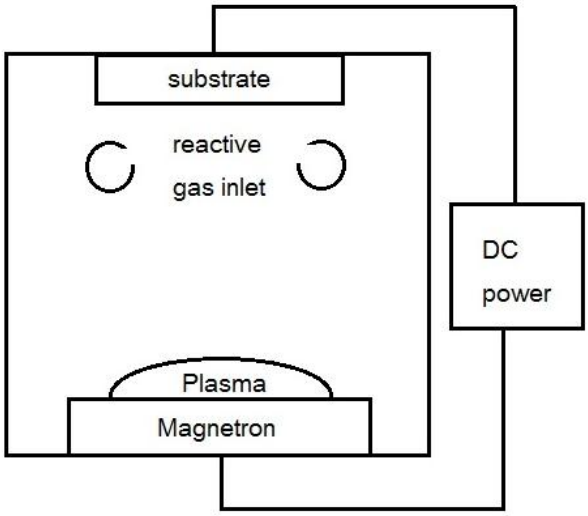

Figure 1-7 The illustration of the reactive magnetron sputtering setup (Kelly & Arnell, 2000)

1.3.4 Spray pyrolysis

It is preferred to produce the spherical nanoparticles that do not aggregate with others and have the narrow size range for the application. Besides, the processing method should also synthesize particles where their size, morphology and composition are under controlled. Typically, the method to synthesize the nanoparticle or thin film could be categorized into two: gas–to–particle conversion and liquid –to –particle conversion. The gas –to–particle conversion is transforming the gas phase particles into solid-state

particles with the process of nucleation and condensation or even coagulation. It is a build-up method. Examples for the gas–to–particle conversion are gas evaporation and sputtering that we have discussed so far. But this method had the drawback of having the difficulties to prepare uniform multicomponent materials (Okuyama & Wuled Lenggoro, 2003).

The other synthesizing method, liquid –to –particle conversion, or so-called spray pyrolysis and aerosol decomposition synthesis (Swihart, 2003) has been taken into account recently. It is a break-down process. The synthesizing process is to deliver the droplet of precursor into the reactor by using nebulizer. Since the reactor is in high temperature, the solvent would evaporate and the remaining solute reacted with the surrounding gases and diffused to precipitate on the substrate. The schematic of how particles formed in the reactor by the spray pyrolysis is shown in Figure 1-8. From the figure, components for the spray pyrolysis instrument are a nebulizer used to disperse the precursor as droplets, carrier gases for carrying droplets, a reactor and the substrate where to collect the final product.

It was shown that the composition of the final product was determined by the stoichiometric ratio of the solute dissolved in the precursor. The final particles size and their size distribution were caused by the size of the droplets, the velocity of the droplets and the concentration of the precursor. Finally, the morphology of the final product was affected by the surrounding gas flow rate, the temperature and the precursor. The carrier gases flow was affected because it influenced the residence time of the solvent evaporation (Okuyama & Wuled Lenggoro, 2003).

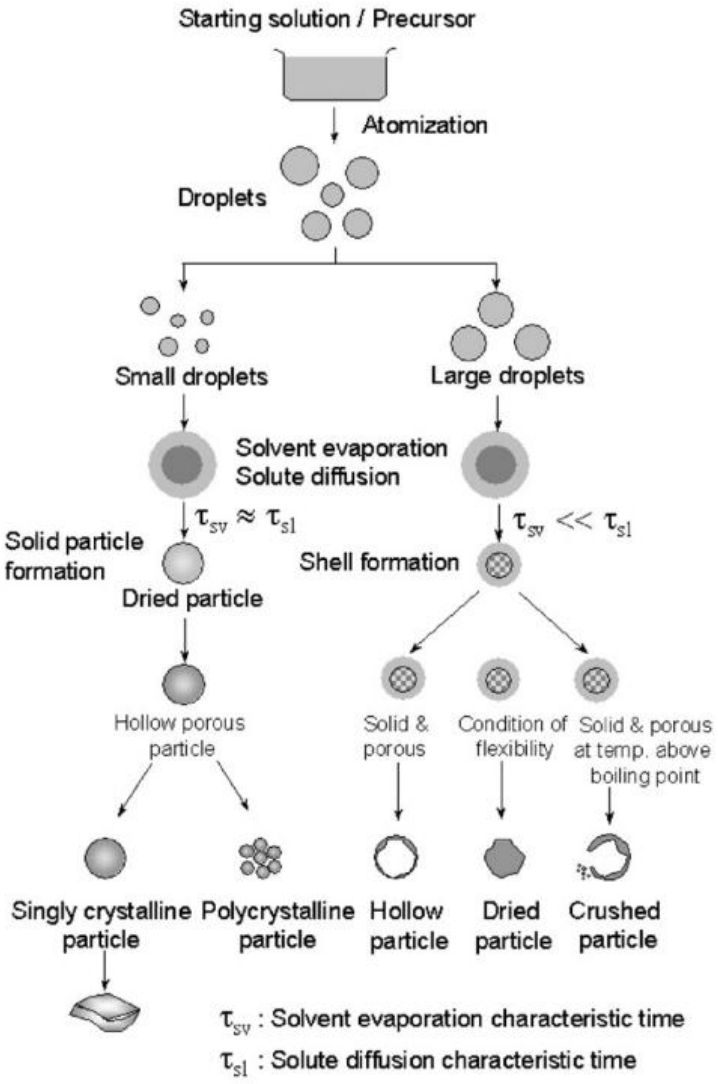

Figure 1-8 The particle formation by using the spray pyrolysis (Okuyama & Wuled Lenggoro, 2003)

1.3.5 Flame spray pyrolysis

Flame aerosols reactors have three categories which are categorized based on the state of precursor and the condition for combustion.

1. Vapor-fed aerosol flame synthesis (VAFS): The vapor-state precursor has been used. In order to process continuously, the precursor should keep supplying to the system.

However, the replacement of the gas state precursor is hard to handle and expensive in the industry point of view (Teoh et al., 2010).

2. Flame-assisted spray pyrolysis (FASP): Since the vapor-state precursor is difficult to replace, the liquid precursor has been used. In this technique, the precursor is aqueous solution in order to prevent volatile usage. But the precursor has the properties of low combustion enthalpy (<50% of total combustion energy) so that the self-sustaining flames could not formed. To be noticed, the combustion enthalpy is equal to combustion rate/ total gas flow. Therefore, the external flame which composed of oxy-hydrogen or oxy-hydrocarbon is required (Teoh et al., 2010).

3. Flame spray pyrolysis (FSP): The liquid-state precursor is used and it has higher combustion enthalpy (>50% of total energy of combustion) so that the flame is self-sustaining. Usually, the organic solvent is used (Teoh et al., 2010).

The flame spray pyrolysis is composed of an atomizer or a nebulizer, a burner and a collecting system. The detail for each component is described in the following.

- Atomizer: The purpose of atomizer is to create droplets. The most common atomizer used in FSP is two-fluid nozzle as illustrated in Figure 1-9 due to the nanoparticles formation. The two-fluid nozzle can help to mix precursor and carrier gas together so that the carrier gas could carry droplets to the substrate (Purwanto, Wang, & Okuyama, 2011).

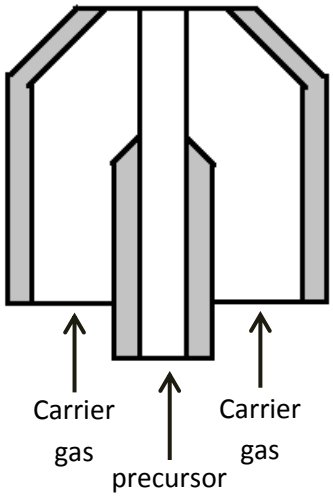

Figure 1-9 The illustration for two-fluid nozzle (Purwanto et al., 2011)

- Burner: There are two types of burner: the diffusion burner and the premixed burner. The diffusion burner does not mix the fuel and the oxidant before encountering flame; on the contrary, the premixed burner mixes the fuel and oxidant (Purwanto et al., 2011). In addition, FSP can generate the self-sustaining flame so that the burner system for it is an ignition source; in other words, the FSP does not need the external flame source. The advantage for it is that it could directly control the particle size by controlling the combustion enthalpy and the metal concentration of the precursor (Teoh et al., 2010).

- Collector: the substrate or filter that the final product can be collected.

Furthermore, the types of precursor have a strong influence on the particle size. The precursors that we used in the FSP usually fall into three kinds: metallorganic precursors, aqueous salt precursors with atomizer and aqueous salt precursors with ultrasonic nebulizers. Among all, the metallorganic precursors and the aqueous salt precursors with atomizer can form nano-sized particles (Purwanto et al., 2011).

Understanding the Mechanism of Particle Formation for FSP

Three different mechanisms for the particle to form in the FSP have been proposed:

1. Gas phase mechanism

The precursor of metallorganic compounds usually forms the particle via the gas phase mechanism. Metallorganic compounds evaporate quickly as soon as they enter the flame zone to form a precursor vapor. In the gas evaporation process, the vapor could collide with the carrier gas to nucleate forming clusters. Besides, vapor could also nucleate on the surface of formed clusters to cause new particles growth. The more clusters are forming the higher the probability is for them to collide with each other and to form strong adhesive (physical) bonds or chemical bonds resulting in coagulation to produce nanoparticles. Finally, those nanoparticles would produce single particles during coalescence process which is the process to aggregate particles in the high temperature zone. If we would like to control the particle size for not aggregate too much particles together, the lower residence time of precursor should be approached; in other words, the flow rate should be higher (Purwanto et al., 2011).

2. One-droplet-to-one-particle (ODOP)

The first step for this mechanism to result in particle formation is evaporating the solvent in order for the solute to disperse in the reactor. Each solute would react with the carrier gas or each other to form particles. Finally, particles undergo sintering and densification process. Since one droplet would form a particle, the size of the particle was usually in the micro-scale.

The particle size for this mechanism can be predicted from the below formula:

$$\mathbf{dp} = \left(\frac{\boldsymbol{Cd^3M}}{\boldsymbol{n\rho}}\right)^{\mathbf{1/3}}$$

dp: average particle size

C: droplet concentration (precursor concentration)

d: droplet diameter

M: molecular weight of the particles

n: stoichiometric ratio

ρ : particle density

From the formula, we can notice the particle size is influenced by the precursor concentration (Purwanto et al., 2011).

3. One-droplet-to-multiple-particles (ODMP)

The steps for forming particles by this mechanism are the same as the one-droplet-to-one-particle. The difference between these two is the precursor. For ODMP mechanism, the precursor contained organic additive which would crack in the sintering process so that each droplet broke down into multiple particles (Purwanto et al., 2011).

Those three mechanisms can be summarized in Figure 1-10.

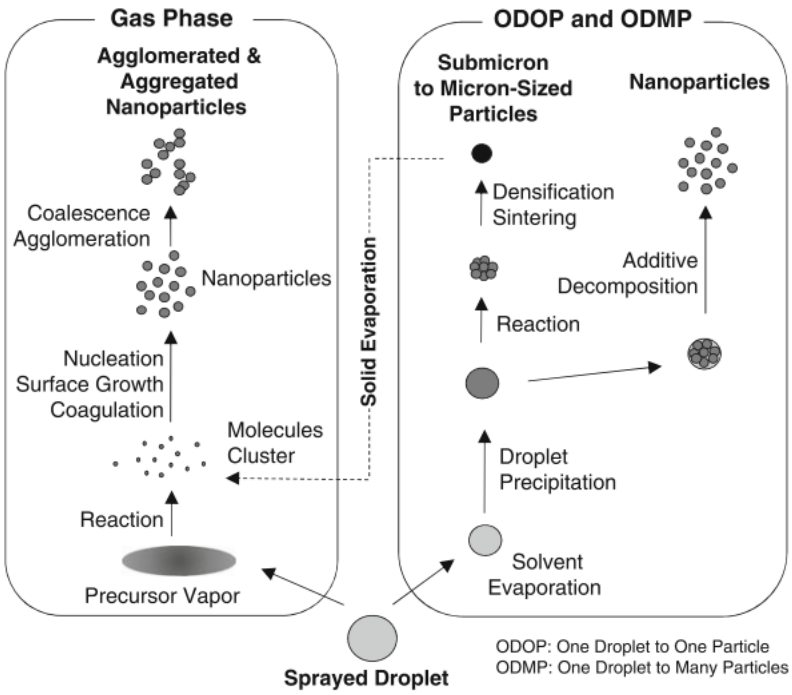

Figure 1-10 The summary of the particle formation for flame spray pyrolysis (Purwanto et al., 2011)

From the mechanism of particle formation above, we knew that the particle size, morphology and crystal structure were strongly influenced by the precursor and the carrier flow. Table 6 summarized the factors that affected the final product in the flame spray pyrolysis processing.

Table 6 The summary of factors affected the final particle (Strobel & Pratsinis, 2007)

Consequence	Factors
Crystal Size	Precursor composition, fuel and oxidant flow rate, burner configuration, size of droplet and flame
Crystal structure	Precursor flow rate and fuel/oxidant flow rate
Crystal morphology	Precursor concentration and fuel/oxidant flow rate

Among all the processing method that we discussed so far, flame spray pyrolysis has the highest processing temperature (so far the highest temperature that has been measured is 2800 K) and the highest gas flow rate. Based on these two factors, the flame spray pyrolysis is the only processing method that can provide very short residence time (in ms scale) in the highest temperature gradient region (Teoh et al., 2010). As we know, the ε – phase is the metastable phase. The condition to synthesize ε – phase is basically following the ODMP mechanism: When the droplet be disperse into the reactor by atomizer, the solvent would evaporate and the tungsten ion in solute would react with the oxygen to form tungsten trioxide nanoparticles. The phases for those tungsten trioxide nanoparticles are the structure of ε – phase due to the large temperature gradient. But when it undergo the sintering process, the residence time for particles to be sintered is short so that it would not have enough time to transform to more symmetric structures and stay at ε – phase. Therefore, the flame spray pyrolysis is the best processing method that we can produce ε – phase at room temperature.

1.4 The application for ε – phase

The application for tungsten trioxide so far are electrochromic devices (Jiao et al., 2012), sensors (L. Wang, Teleki, Pratsinis, & Gouma, 2008) and photocatalyst (Zhang, Huo, Hu, & Chu, 2010). It has been studied that ε – phase has the highest selectivity for acetone which could be use in the hand-held breath acetone monitor (L. Wang et al., 2008).

Our exhaled breath is not only composed of CO_2, N_2, O_2 and H_2O but also some small amount of inorganic molecules and volatile organic compounds (VOCs); for example, NO, NH_3, CO, acetone, methanol and ethanol. It has been found that the concentration for those

molecules was relating to the health conditions. Therefore, these gases are called biomarkers in the breath (Lisheng Wang's dissertation).

For example, people who drink alcoholic beverages would have the concentration of ethanol in the range of 13 ppb to 1000 ppb in their exhaled breath compared with the concentration range from 27 ppb to 153 ppb of non-drinking people.

Acetone is also one of the biomarker in our breath. It has been found that the concentration of acetone in the breath for a health person is less than 0.8 ppm, for a diabetic patient is larger than 1.8 ppm and for the patients of diabetic ketoacidosis is larger than 500 ppm (Manolis, 1983; Tassopoulos, Barnett, & Russell Fraser, 1969). It also been proved that the measuring of acetone in breath was more sensitive than blood glucose for the condition of controlling the insulin levels (Manolis, 1983). This is why a breath acetone monitor may be best for the control of diabetes.

The Principle of Ferroelectric Poling

The ε – phase of WO_3 has ferroelectric properties so that it is expected to undergo ferroelectric poling under an applied electric field. Ferroelectric poling can be seen at below the Curie temperature, called" normal poling" and above curie temperature, called" high poling". For the high poling, a residual internal bias field has been generated and it has opposite direction as the external electric field when it cooled down under the Curie temperature. In the case of normal poling, the internal bias field has the same direction as the external electric field (Kiyoshi, 1993). It is known that the ferroelectric poling is dependent on the thickness of the ferroelectric material. The thicker the ferroelectric material, the direction of ferroelectric poling would be influenced by the external electric field. When the

thickness goes down, the ferroelectric poling is affected by the surrounding molecules (Fong et al., 2006).

As described in section 1.2.2, ε – WO_3 has non-vanishing dipole moment in z direction so that creating the polar surface of ε – WO_3 (Claudine, 2000). Acetone gas consists of polar molecules which would be attracted by the dipole surface of ε – WO_3 with electrostatic interaction (Yun & Altman, 2007). Thus, ε –WO_3 is the materials of choice to develop an acetone breathalyzers used to monitor the insulin levels in order to control diabetics.

1.5 Research Statement

From the above background information, the ε – WO_3 is the material that used in the hand-held breath acetone sensor which could be used to effectively monitor the insulin levels of diabetics. In order for ε – WO_3 to maintain its structure in the sensors under different working temperature, the phase should exhibit stability even at high temperatures. In other words, the ε – phase should be fully crystalline at high temperature.

The technique that has developed so far showed that the pure ε – WO_3 could be existed at room temperature but it would undergo the phase transformation to γ – phase after the heat treatment. On the contrary, the doped WO_3 showed that the ε – WO_3 could be stabilized after the heat treatment. The highest percentage of ε – WO_3 that still presented after the heat treatment showed in the literature so far is 87 %. However, the doping of WO_3 may be harmful to the sensor due to the dopant is toxic compound.

This thesis will focus on producing higher percentage of pure ε – WO_3 nanoparticles that are fully crystalline and exhibit phase stability at high temperatures. The synthesizing method that we used is flame spray pyrolysis because it has higher temperature gradient and

rapid cooling rate so that it has higher possibility to produce the metastable phase of ε – WO_3.

Chapter 2 Experimental Details

In this chapter, the experimental processing and the characterization methods for this thesis will be introduced. The experimental processing is flame spray pyrolysis and the characterization methods are scanning electron microscopy (SEM), X-ray diffraction (XRD), transmission electron microscopy (TEM), Raman spectroscopy and ferroelectric testing.

2.1 Flame Spray Pyrolysis

The flame spray pyrolysis that used in this thesis is TETHIS nps10 nanoparticle synthesizer housed in our lab. The equipment composed of precursor unit, the burner unit and the collection unit. The precursor portion used a syringe to take the solution from the beaker. The amount of the taken precursor was controlled by the computer. In this thesis, the amount of taken precursor has been set to 30 ml and the precursor solutions are summarized in Table 7.

Table 7 Precursor solutions used in this thesis

Sample Number	Solute	Solvent	Concentration
A	Tungsten (VI) isopropoxide	isopropanol	0.22 M
B	Tungsten (VI) isopropoxide	6:1 (volume ratio) mixture of xylene and isopropanol	0.12 M
C	Tungsten (VI) isopropoxide	5:1 (volume ratio) mixture of xylene and isopropanol	0.22 M
D	Tungsten (VI) isopropoxide	xylene	0.15 M
E	Tungsten (VI) isopropoxide	xylene	0.22 M
F	Tungsten (VI) isopropoxide	xylene	0.3 M

All chemicals is provided as following: tungsten (VI) isopropxide (99%, All-Chemie LTD.), isopropanol (Sigma-Aldrich, 99.5 %), xylene (Sigma-Aldrich, 98.5 %)

The burner unit composed of flame, dispersion gas and the nozzle which used to atomized the precursor into droplet. The flame contained 1.5 sl/min of methane and 3.2 sl/min of oxygen. 5 sl/min of oxygen served as the dispersion gas was fed into the reactor. The precursor flow rate was 5 ml/min and no sheath gas has been used in this study. The collecting system for this equipment was glass fiber filters (Whatman).

2.2 Characterization Methods

2.2.1 Scanning electron microscopy (SEM)

The scanning electron microscopy used electrons as the source so that we can get higher resolution image to study the composition and the surface of the sample. The compositions of SEM are electron gun served as source, lens of condenser and objective used to focus the beam into a small probe on the specimen and specimen. The electron gun, which could be filament or field emission, produces electron beam and electrons go down through the column toward the specimen. During their path, a lot of lenses are on their path in order to focus the beam to create a small probe size on the specimen.

The signals that we can get from scanning electron microscopy are backscattered electrons and secondary electrons. Backscattered electrons are produced from the interaction of electron beam and the nucleus of the atom in the specimen. Since it is an elastic interaction, the energy of the backscattered electrons does not have a significant changing from the electron beam but only direction changed. Because the backscattered electrons interact with the nucleus,

it could give us the information of the specimen composition. On the contrary, when the electron beam interacts with electrons in the specimen atom, the inelastic interaction would happen causing the energy transfer. The secondary electron usually has energy less than 50 eV. The escaping depth of the secondary electron is 5 nm to 50 nm which could give us the information of the surface information of the specimen.

In this thesis, the SEM is used to study the morphology of our samples. The SEM image was obtained from the facility of JEOL 7600F High Resolution Analytical SEM in Brookhaven National Laboratory (BNL) operated at the voltage of 50 kV

2.2.2 Transmission electron microscopy (TEM)

Transmission electron microscopy, same as scanning electron microscopy, uses the electron as the source but it can provide higher resolution so that we can study the crystal size, crystal morphology and crystal structure of our sample. The electron source and column configuration for TEM is same as SEM. The difference between these two electron microscopies is that TEM used thin sample so that the electron beam can penetrate through the sample. There are two images that we can get from TEM: images and diffraction pattern. If you take the lens above the specimen as the objective lens, the image plane can give you images. It is used to study the crystal size and crystal morphology of the specimen. On the other hand, if you take the back focal plane as the objective lens, diffraction patterns are be collected and gave us the information of the crystal structure of our specimen.

In this studied, the crystal size can be studied from the TEM images. JEOL's JEM-1400 in BNL is used in this thesis.

2.2.3 X-ray Diffraction (XRD)

X-ray diffraction is the technique that commonly used to study the crystal structure and analyze whether your sample is crystalline or not. By Applying the sample with a monochromatic X-ray beam with a wavelength λ at a certain angle θ, the diffraction could be detected only when it is satisfied with Bragg's Law: $2d\sin\theta = n\lambda$ where d is the distance between adjacent crystal planes. Because different crystal has different d-spacing, the diffraction intensity and diffraction angle would be different.

Usually this technique is applied X-ray within a certain range of angle. With the various angle, we can get the diffraction intensity at that certain angle. By comparing the plot of diffraction intensity and diffraction angle with standard Joint Committee on Powder Diffraction Standards (JCPDS), we can know the crystal structure of the sample.

In this studied, XRD is used to study the phase of the samples. Rigaku's Ultima III in BNL has been operated at 40 kV and 30 mA under the wavelength of Cu Kα radiation which is 1.54184 Å.

2.2.4 Raman Spectroscopy

Raman spectroscopy is used to study the vibrational state of the photon. It has been known that the vibrational state is specific to certain chemical bond; in other words, the vibrational state is the fingerprint for the chemical bond. Therefore, the Raman spectroscopy can be used to study the local structure and the chemical composition for the sample.

When light interacts with the sample, the photon could be absorbed or scattered. When we focus on the scattering process, the photon could be elastic scattering (Rayleigh scattering) or

inelastic scattering (Raman Effect). Most photon would undergo elastic scattering but small portion of them would undergo Raman Effect. Raman Effect is to distort the electron clouds of atom and form virtual state when the light interacts with the sample. Virtual state is short life and not stable so that the photon would radiate again and go back to vibrational state. Since the Raman scattering is inelastic scattering, some energy would loss during the scattering process. The amount of the energy loss is strongly sensitive to the chemical bond so that the frequency becomes the fingerprint for the chemical structure.

In our study, the Raman spectroscopy is used to study the phase for our sample. Compared with XRD, Raman spectroscopy provides more accurate phase information because it is sensitive to the small shift of tungsten position. From the section 1.1.2, the different phases of WO_3 only have a small shift of the tungsten atom. Based on the tungsten atom local chemical structure, we could study the phase structure of our sample.

In this thesis, WiTec Alpha confocal Raman microscopy in BNL has been conducted. The green light laser of the wavelength of 532 nm has been used for excitation.

2.2.5 Ferroelectric Testing

Ferroelectric testing is applying negative and positive voltage pulses between two electrodes while measuring the capacitance and dielectric loss. It is known that for a ferroelectric material one can observe the hysteresis loop in polarization versus voltage curve and butterfly shape in capacitance versus voltage plot as shown in Figure 2-1.

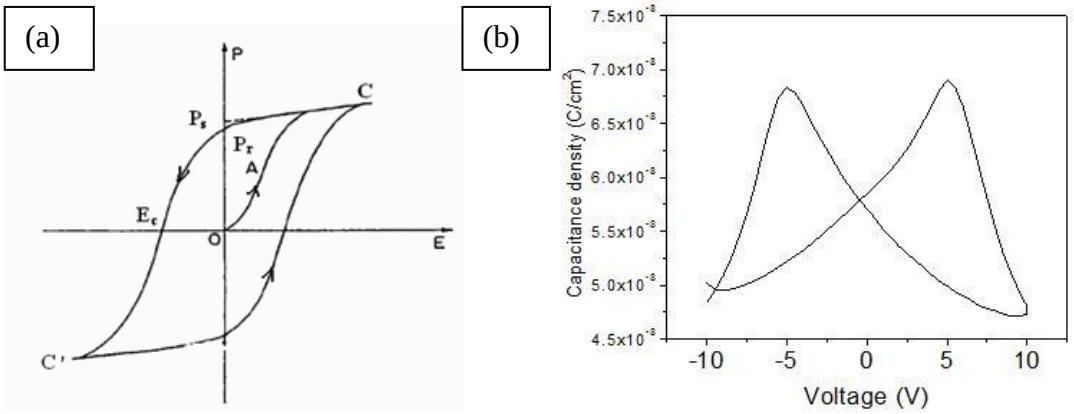

Figure 11 Typical ferroelectric materials showed (a) hysteresis loop that Ps stands for spontaneous polarization, Pr stands for remnant polarization and Ec stands for coercive field (b) butterfly curve (Lallart, 2011; Zhao, Qu, Ye, & Xiong, 2008)

In our study, the device used for the ferroelectric testing is displayed in Figure 2-2.

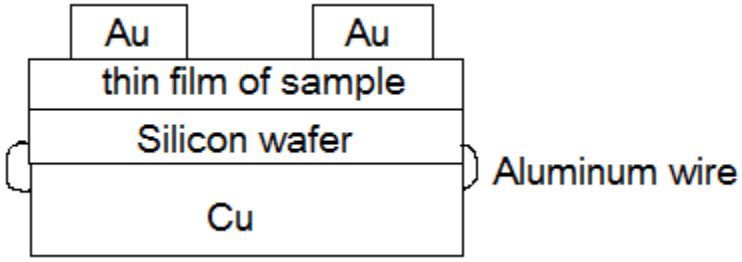

Figure 12 The schematic figure of the device for ferroelectric testing (courtesy of Dr. Fernando Camino from BNL and Dr. Matthew Dawber in Stony Brook University Department of Physics)

The construction of the device involved:

First, the silicon wafer should have low resistivity so that it is conductive. The silicon wafer used in this studied was around 150 Ω. Then the silicon should undergo the cleaning process so that it would not contain the impurity between silicon and the thin film. The cleaning process for silicon wafer was done as the following procedure:

1. Soaking silicon wafer in acteone and sonication for 20 minutes.
2. Rinsing the silicon wafer with DI water.
3. Soaking silicon wafer in methanol and sonication for 20 minutes.
4. Rinsing the silicon wafer with DI water.
5. Soaking silicon wafer in DI water and sonication for 20 minutes.
6. Placing the silicon wafer in oven under 100 ℃ to dry out.

Second, dissolved the powder of the sample in ethanol and sonication for 15 minutes to make sure the powder was dispersing around the solution. The sample we used for the ferroelectric testing was the as-synthesized sample D3 that described in Lisheng Wang's dissertation. After sonication, drop coating the solution on the silicon wafer to create a thin film.

Third, coated gold with the mask on the thin film by using thermal/ebeam evaporator. The diameter of each gold island was 1 mm and the thickness was 100 nm. The gold was served as the top electrode. Then, connecting the silicon wafer with copper sheet by stapling multiple aluminum wires around their edges so that the copper was served as our bottom electrode.

Lastly, use two probes on the probe station to apply electrical field. One probe connected to the bottom electrode and the other connected to the top electrode. Applied the electrical field from -2 V to 2 V and frequency for 1000 kHz to the device and measured the capacitance and dielectric loss to determine its electrical properties.

Chapter 3 Result and Discussion

3.1 As-synthesized pure tungsten trioxide nanoparticles

3.1.1 Particle size and morphology

The particle size of the as-synthesized WO_3 is hard to deduce from the SEM image of Figure 3-1 as the individual particles are hard to distinguish. Rather, one can see particle aggregating together to form multiple large round particles. From the TEM images shown in Figure 3-2, particles are sphere-like shape and the size is in the range of 10 nm to 30 nm among different precursor. It shows the same result that the type of precursor will influence the size of particle. (Purwanto et al., 2011) On the other hand, the SAED patterns for different precursor shows the almost continuous ring patterns also indicate the crystal is in nano-scale and polycrystalline. The SAED pattern in Figure 3-3 for sample A showed the ring is close to continuous compared with sample C and sample E is because the particles size of sample A is smaller.

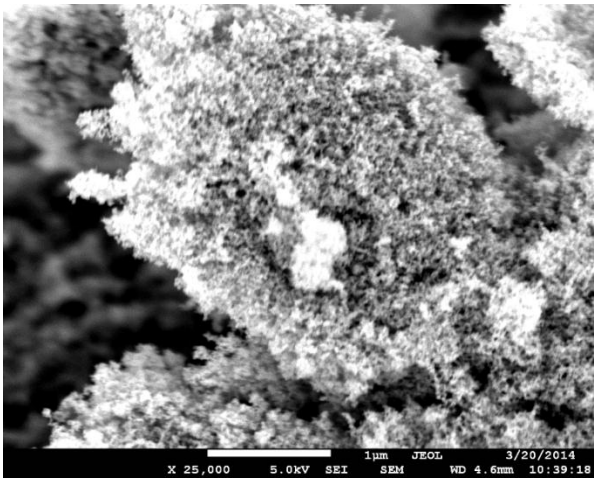

Figure 13 SEM image for Sample A

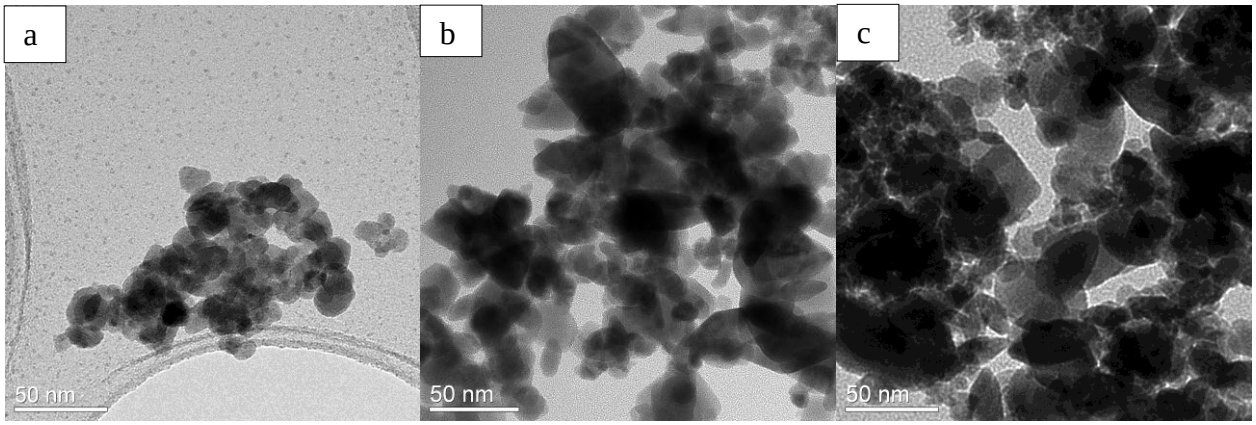

Figure 14 TEM images for (a) Sample A (b) Sample C (c) Sample E

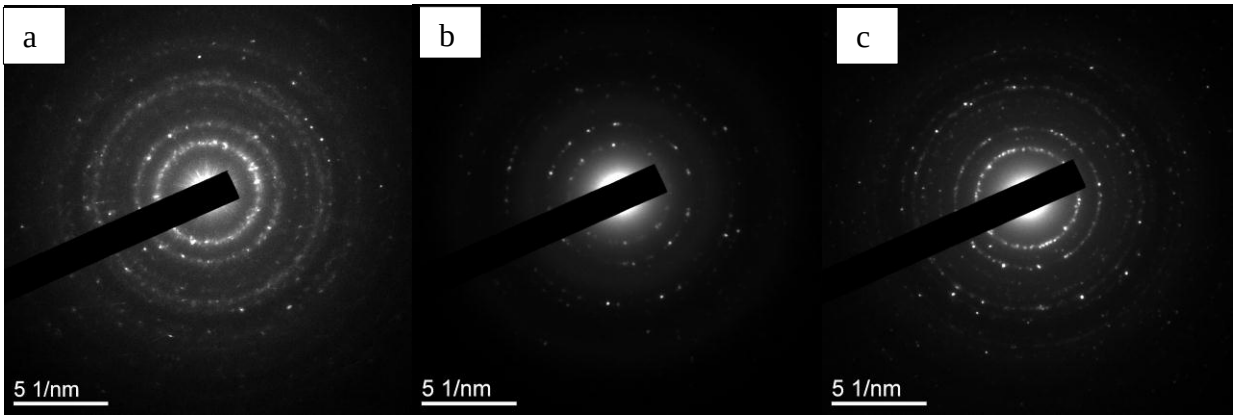

Figure 15 SAED pattern for (a) Sample A (b) Sample C (c) Sample E

3.1.2 Phase determination

As described in section 2.2, XRD is the most common technique to be used in analyzing structures; however, it is hard to distinguish the phase in the nanocrystalline WO_3. The reason is that the characteristic peaks for different structures are closely spaced.

In this study, XRD data were used to confirm the structure of the as-spray samples is WO_3 instead of the other oxide structure for tungsten. Figure 3-4 shows the XRD data among all different types of precursor. All XRD spectra match with the JCPDS file with monoclinic ε - phase.

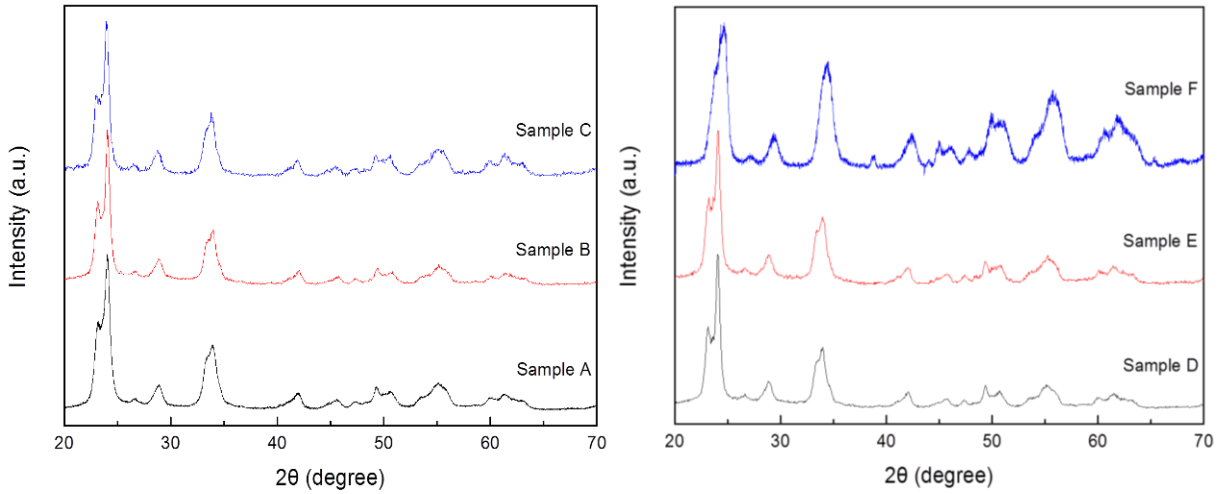

Figure 16 XRD data for all samples shows that as synthesized samples match with ε-phase

The Raman spectra can provide more accurate phase information than XRD because it is more sensitive to the changes in the local structure. Based on the preliminary study, the peaks present at 272, 324, 715 and 805 cm^{-1} belong to γ – phase and peaks at 203, 272, 303, 370, 425, 642, 688 and 805 cm^{-1} belongs to ε – phase (Lisheng Wang's dissertation). Analyzing the Raman spectra of all samples, it is showed that Sample A has γ – phase predominately and almost no ε – phase as the characteristic peaks of ε – phase are at 642 and 688 cm^{-1} but are not observed and the intensities for 303 and 370 cm^{-1} are low. Sample B contains both ε – phase and γ – phase with ε – phase being more abundant. Note the relatively higher intensity at 688 cm^{-1} than 715 cm^{-1}. Sample C also showed the coexistence of ε – phase and γ – phase but the portion for γ – phase is slightly higher due to the higher intensity of 715 cm^{-1} than 688 cm^{-1}. Sample D and Sample E showed the same condition as Sample A that most of the phase in the sample is γ – phase. Lastly, Sample F showed that ε – phase and γ – phase coexisted and shared the same percentage in the sample because the intensity for 715 cm^{-1} and 688 cm^{-1} are almost the same.

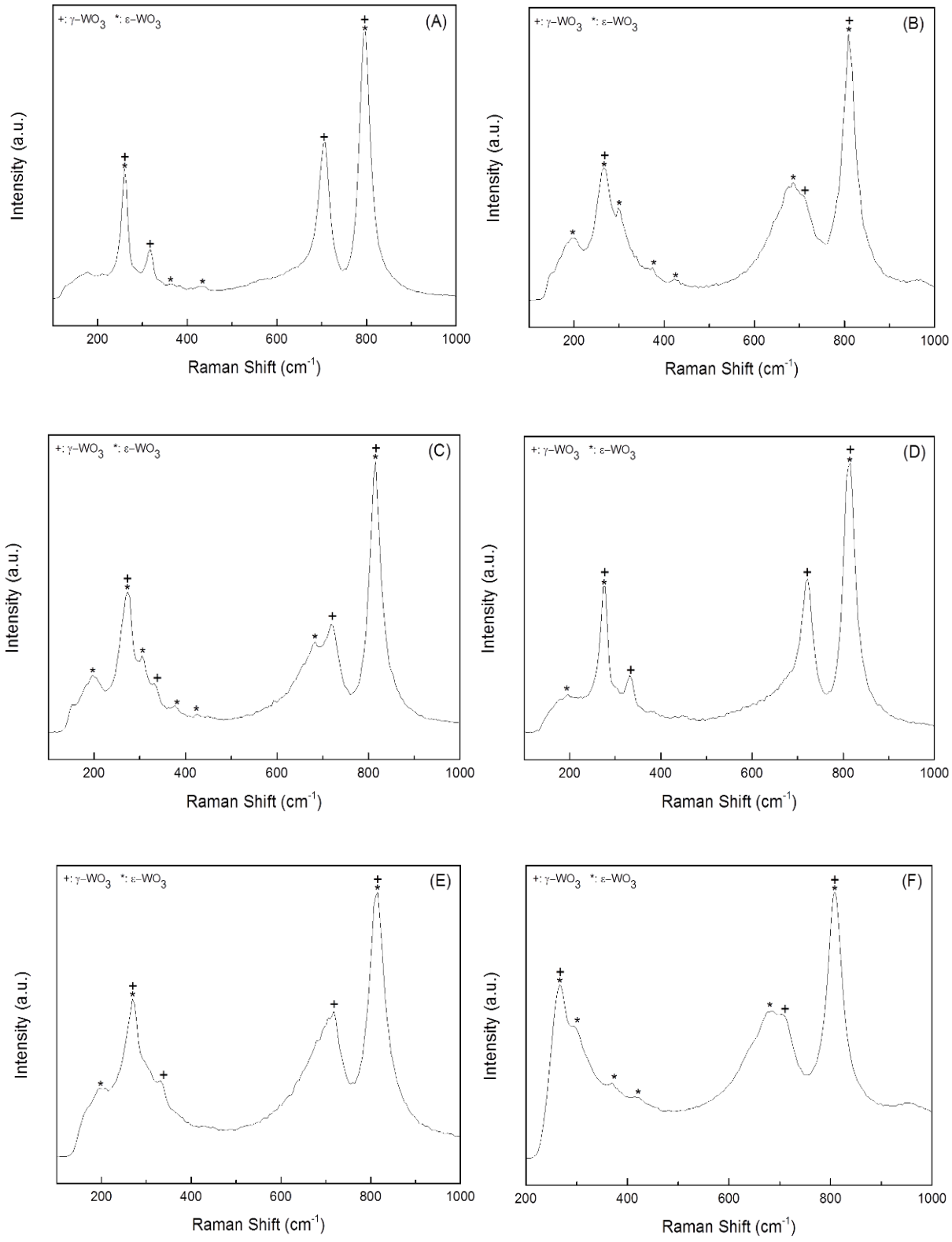

Figure 17 Raman spectra for (A) Sample A (B) Sample B (C) Sample C (D) Sample D (E) Sample E (F) Sample F

When comparing samples D, E and F, it is derived that the increasing concentration of xylene resulted in higher volume fraction of the ε – phase present. It may be due to the low solubility of isopropoxide in xylene causing the ε – phase to remain in the sample. Besides, Sample B and C also showed that adding xylene into the isopropanol can help ε – phase preserve.

3.2 The influence of heat treatment

The heat treatment at 500 ℃ for 8 hours has been done for all as-synthesized samples. The purpose for doing the heat treatment is to assess the phase stability of the powders.

The XRD result can be seen in Figure 3-6 that showed Sample A to Sample E undergo phase transformation to γ – phase by matching the JCPDS files of γ – phase. However, it is interesting to notice that Sample F does not undergo phase transition but matches with ε – phase.

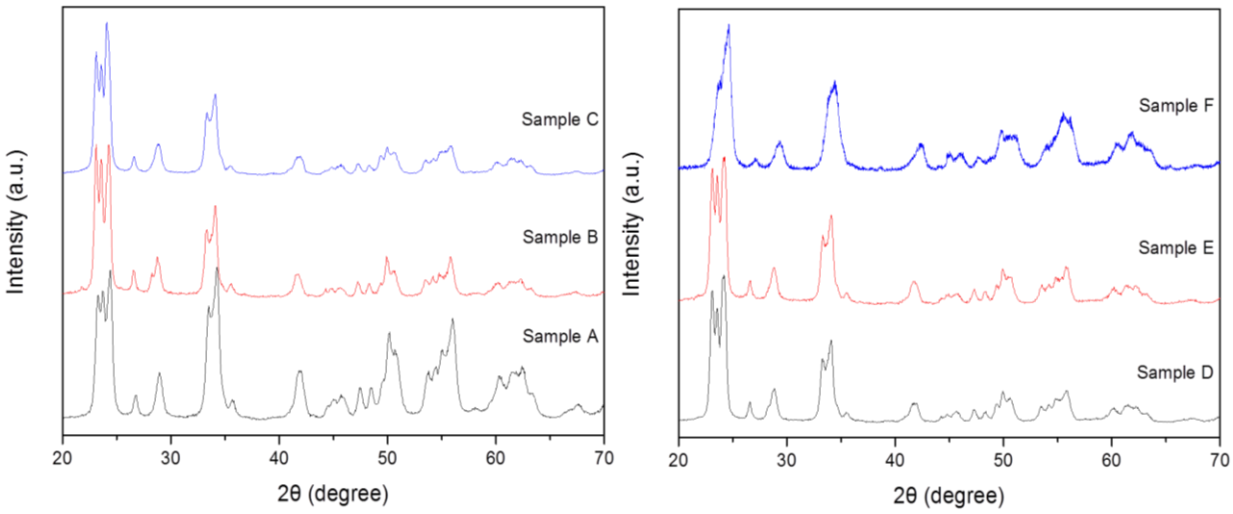

Figure 18 XRD result for samples after heat treatment

The Raman spectra (as shown in Figure 3-7) showed that all samples have the coexistence of ε – phase and γ – phase and most of them showed that the γ – phase is predominant due to the higher intensity at 715 cm^{-1}. Interestingly, Sample A and Sample F

showed that ε – phase and γ – phase have approximately the same percentage in the sample. In addition, focusing on Sample F and comparing the Raman data before and after the heat treatment, it also indicated that the phase does not undergo any change upon the heat treatment.

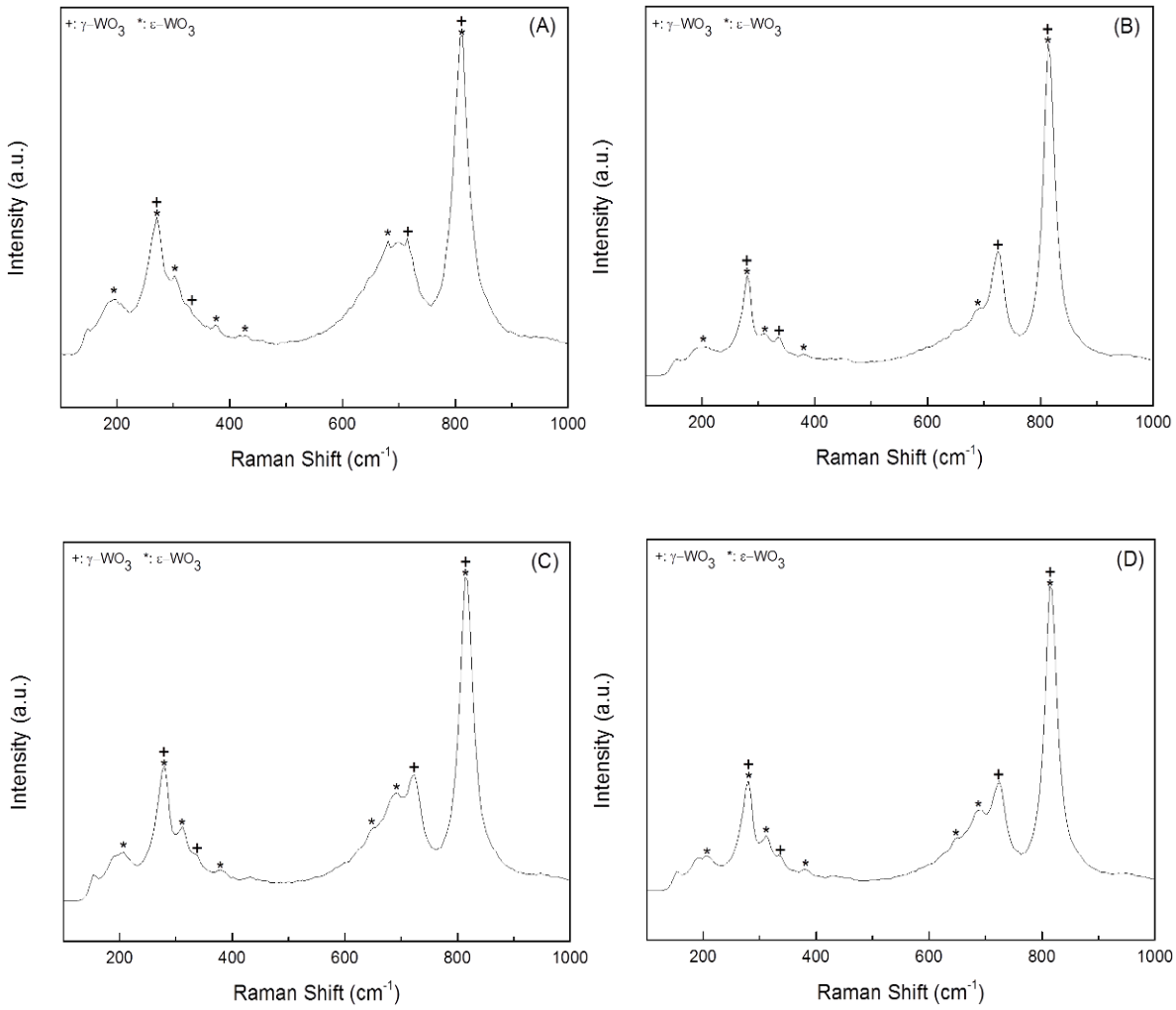

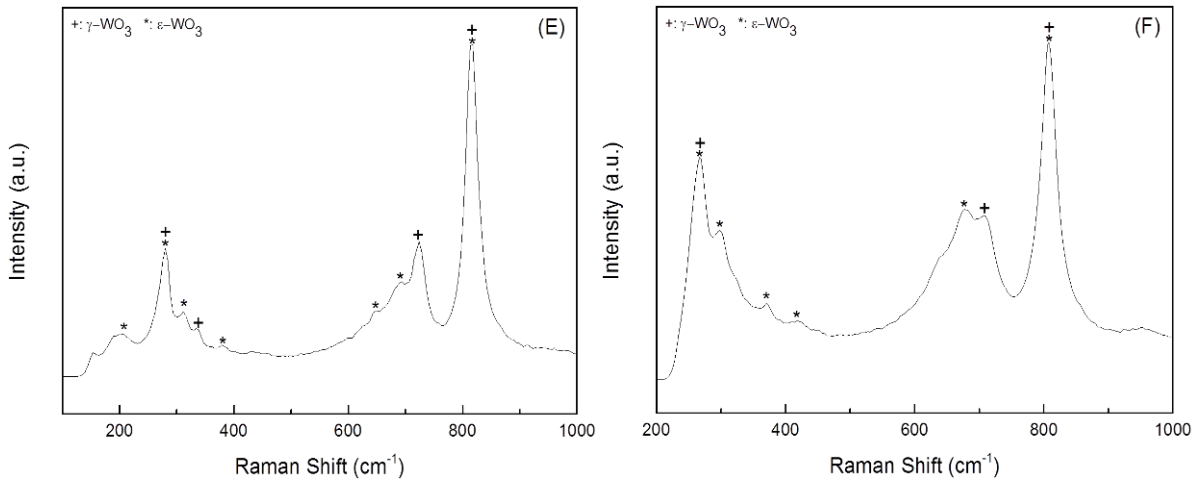

Figure 19 Raman spectra for samples after heat treatment

TEM analysis for sample F before and after the heat treatment was used to estimate the grain size and to obtain diffraction patterns as shown in Figure 3-8. From the TEM images, the grain size does not undergo a significant size change before and after the heat treatment. The smallest grain size before heat treatment is 15 nm and after heat treatment is 20 nm. Besides, it also showed the bimodal particle size distribution in the range of 15 nm to 50 nm. Based on preliminary study, the smaller grain size would tend to be in ε – phase and larger grain size tend to be γ – phase (Lisheng Wang's dissertation). Therefore, the coexistence of ε – phase and γ – phase in Sample F is resolved. The SAED pattern also real the same result that rings matched with the crystal plane (110) of ε – phase and (024) of γ – phase.

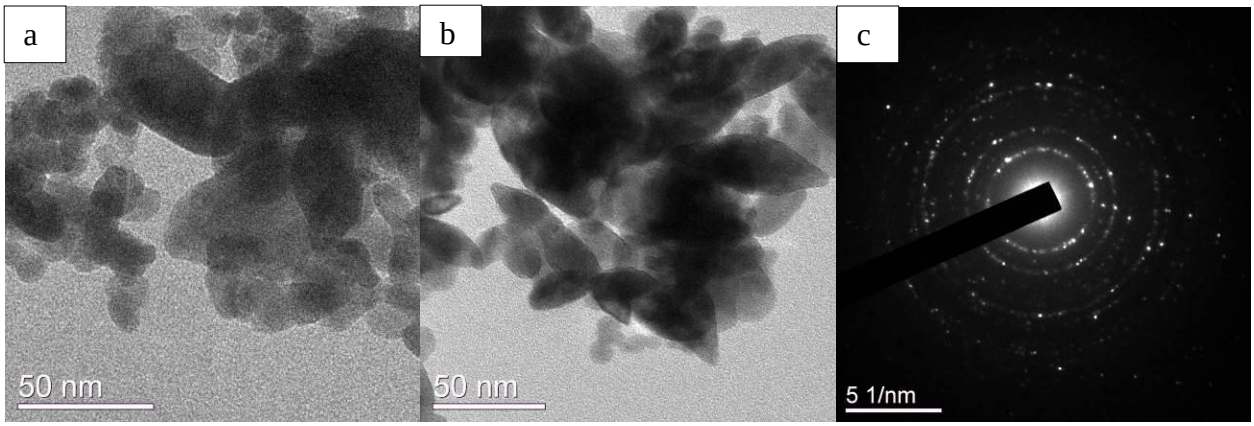

Figure 20 TEM image (a) before heat treatment (b) after heat treatment and (c) SAED pattern after heat treatment

The reason that the xylene could stabilize the ε-phase after high temperature treatment could be because the evaporation rate for xylene is higher than that for isopropanol. Based on computational models to predict the dynamics of flame spray pyrolysis, the height above the burner for ethanol to completely evaporate is higher than 1-propanol (Gröhn, Pratsinis, & Wegner, 2012). Besides, the starting point for the solvent to evaporate is different because it is governed by its boiling temperature. The height above the burner that the solvent can reach is determined by mass transfer equations. Since the ethanol has lower boiling point and lower mass, the range that it could evaporate is larger than 1-propanol (Gröhn et al., 2012).

For the case of xylene and isopropanol, xylene has higher boiling point (138.5 ℃) and higher mass than isopropanol. Therefore, the height above the burner that xylene could reach is lower than isopropanol; in other words, xylene evaporates faster than isopropanol. As a result, when the solute undergoes the evaporation could experience higher temperature gradient causing the metastable phase to nucleate. This is consistent with Lisheng Wang's explanation for the nucleation and growth for the ε-phase.

3.3 Ferroelectric Testing

The dielectric loss versus voltage tells us that the device has some electric properties as shown in Figure 3-9 but the capacitance versus voltage does not shown the typical butterfly curve indicated that our device did not have the ferroelectric properties be detected.

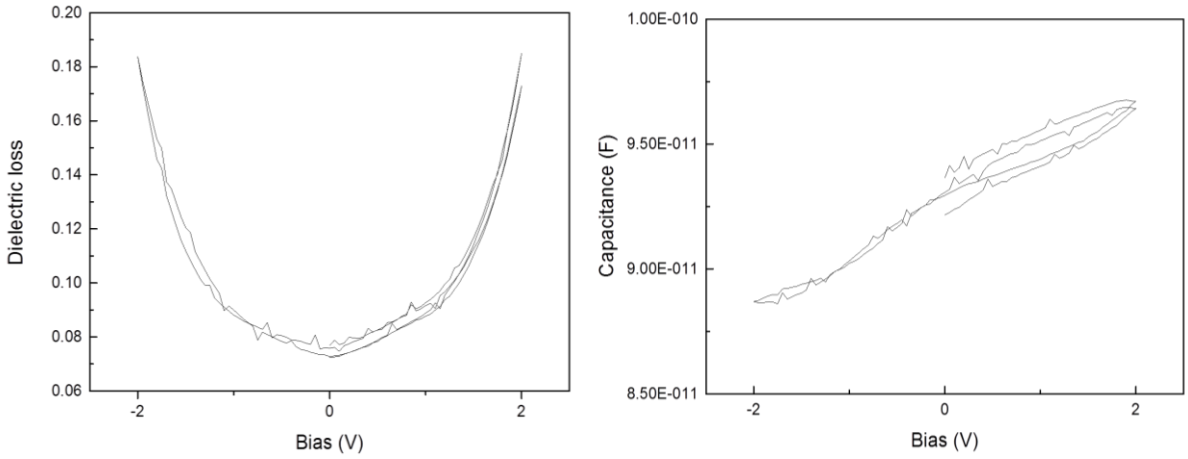

Figure 21 The plot for capacitance and dielectric loss versus voltage

The reasons that we could not detect the ferroelectric properties in our ε -phase sample are: (I) either due to device design limitations or (II) the critical nanoparticle size for detecting ferroelectric properties. Regarding the device limitation, our technique utilized a parallel-plate capacitor which has the area equal to that of the top electrode and the thickness is equal to the thickness of the thin film (Lang et al., 2013). In our case, the top electrode area is large and the thickness of the film is too small so that the capacitance of this capacitor is really large. The consequence would be that it needs more energy to transport the charge from one plate to the other one. As a result, a higher voltage needs to be applied in order to provide higher energy but also run a higher risk for current leakage to occur. Besides, the film for our device is too thin so that may be the current leakage anywhere due to various defects. Therefore, the ferroelectric

properties for our material would be hard to detect using this set-up. The alternative way to improve is using a mechanical press and shape the powder into solid disks followed with the smaller top electrode (around micrometer scale). This is recommended for future studies.

On the other hand, it has been proven that the particle size and film thickness would affect the ferroelectric properties. $BaTiO_3$, a common ferroelectric material, has been studied at the nanoscale and it was found that its ferroelectric properties change with crystal size. It was shown that the ferroelectric properties would disappear for grain sizes below 40 nm (Mangalam, Ray, Waghmare, Sundaresan, & Rao, 2009). There are two factors that influence the ferroelectric critical size: surface energy and screening energy (Vladimir, 2006). Surface energy is from the surface charge and the screening energy is from the screening charge which is resulting from the electrostatic interaction. When the particle size decreases or the thickness of the film becomes thinner, the surface energy or the screening energy will increase. As long as one of these two energies is higher than the lattice energy, the ferroelectricity would disappear (Vladimir, 2006). Since the sample used in our test has the grain size around 15 nm, the ferroelectricity may disappear so that we could not detect the ferroelectric properties although it has been proved ε – phase is dominated in the sample.

Theoretical studies on nanoparticles have suggested that this critical size depends on the material. For example, the critical size for $BaTiO_3$ is 44 nm (Zhong, Wang, Zhang, & Qu, 1994). Therefore, it will be interesting to calculate the critical size for ε-WO_3 using this heuristic approach and this is proposed for future work.

Chapter 4 Conclusion and Future Work

Flame spray pyrolysis allowed us to synthesize WO_3 nanopowders with a controlled phase distribution. In this thesis, it showed that the use of xylene as solvent improved the phase stability in our nanoparticles before and after the heat treatment. This result provides the possibility that the material obtained may be used to develop the next generation of acetone hand-held breathalyzer.

In the aspect of future work, the hypothesis for the higher evaporation rate solvent could stabilize the phase needs to be further confirmed by mixing the tungsten isopropoxide with different organic solvent. In addition, regarding the ferroelectric testing for nanocrystalline ε-phase, the thicker thin film for the testing device and the micro-scale top electrode should be modified for further testing as well as the calculation for ferroelectric critical size of ε-phase.

Reference

Arai, M., Hayashi, S., Yamamoto, K., & Kim, S. S. (1990). Raman studies of phase transitions in gas-evaporated WO3 microcrystals. *Solid State Communications, 75*(7), 613-616. doi: http://dx.doi.org/10.1016/0038-1098(90)90429-F

Cazzanelli, E., Mariotto, G., Vinegoni, C., Kuzmin, A., & Purans, J. (1999). Color centres and polymorphism in pure WO3 and mixed (1−x)WO3−y·xReO2 powders. *Ionics, 5*(5-6), 335-344. doi: 10.1007/BF02375997

Cazzanelli, E., Vinegoni, C., Mariotto, G., Kuzmin, A., & Purans, J. (1999). Low-Temperature Polymorphism in Tungsten Trioxide Powders and Its Dependence on Mechanical Treatments. *Journal of Solid State Chemistry, 143*(1), 24-32. doi: http://dx.doi.org/10.1006/jssc.1998.8061

Claudine, N. (2000). Polar oxide surfaces. *Journal of Physics: Condensed Matter, 12*(31), R367.

Ekhard, K. H. S., Stephan, R., Frank, P., Darryl, M., Kevin, S. K., Thomas, H., & Martin, T. D. (1997). Crystal structure and paramagnetic behaviour of epsilon WO3-x. *Journal of Physics: Condensed Matter, 9*(31), 6563.

Filho, A. G. S., Filho, J. M., Freire, V. N., Ayala, A. P., Sasaki, J. M., Freire, P. T. C., . . . Gomes, U. U. (2001). Phase transition in WO3 microcrystals obtained by sintering process. *Journal of Raman Spectroscopy, 32*(8), 695-699. doi: 10.1002/jrs.727

Fong, D., Kolpak, A., Eastman, J., Streiffer, S., Fuoss, P., Stephenson, G., . . . Rappe, A. (2006). Stabilization of Monodomain Polarization in Ultrathin PbTiO3 Films. *Physical Review Letters, 96*(12), 127601.

Gröhn, A. J., Pratsinis, S. E., & Wegner, K. (2012). Fluid-particle dynamics during combustion spray aerosol synthesis of ZrO2. *Chemical Engineering Journal, 191*(0), 491-502. doi: http://dx.doi.org/10.1016/j.cej.2012.02.093

Hayashi, S., Sugano, H., Arai, H., & Yamamoto, K. (1992). Phase Transitions in Gas-Evaporated WO 3 Microcrystals: A Raman Study. *Journal of the Physical Society of Japan, 61*(3), 916-923. doi: 10.1143/JPSJ.61.916

Hirose, T. (1980). Structural Phase Transitions and Semiconductor-Metal Transition in WO3. *Journal of the Physical Society of Japan, 49*(2), 562-568. doi: 10.1143/JPSJ.49.562

Jiao, Z., Wang, J., Ke, L., Liu, X., Demir, H. V., Yang, M. F., & Sun, X. W. (2012). Electrochromic properties of nanostructured tungsten trioxide (hydrate) films and their applications in a complementary electrochromic device. *Electrochimica Acta, 63*(0), 153-160. doi: http://dx.doi.org/10.1016/j.electacta.2011.12.069

Kaito, C., Kimura, S., & Saito, Y. (1999). Growth mechanism of smoke particles. In T. Nishinaga, K. Nishioka, J. Harada, A. Sasaki & H. Takei (Eds.), *Advances in the Understanding of Crystal Growth Mechanisms* (pp. 235-244). Amsterdam: Elsevier.

Kelly, P. J., & Arnell, R. D. (2000). Magnetron sputtering: a review of recent developments and applications. *Vacuum, 56*(3), 159-172. doi: http://dx.doi.org/10.1016/S0042-207X(99)00189-X

Kiyoshi, O. (1993). Normal Poling and High Poling of Ferroelectric Ceramics and Space-Charge Effects. *Japanese Journal of Applied Physics, 32*(9S), 4241.

Koch, C. C. (1997). Synthesis of nanostructured materials by mechanical milling: problems and opportunities. *Nanostructured Materials, 9*(1–8), 13-22. doi: http://dx.doi.org/10.1016/S0965-9773(97)00014-7

Kuzmin, A., Purans, J., Cazzanelli, E., Vinegoni, C., & Mariotto, G. (1998). X-ray diffraction, extended x-ray absorption fine structure and Raman spectroscopy studies of WO3

powders and (1-x)WO3-y.xReO2 mixtures. *Journal of Applied Physics, 84*(10), 5515-5524. doi: 10.1063/1.368596
Lallart, M. (2011). *Ferroelectrics: Physical Effects*: InTech.
Lang, S. B., Tofail, S. A. M., Kholkin, A. L., Wojtaś, M., Gregor, M., Gandhi, A. A., . . . Plecenik, A. (2013). Ferroelectric Polarization in Nanocrystalline Hydroxyapatite Thin Films on Silicon. *Sci. Rep., 3*. doi: 10.1038/srep02215
Malin, B. J., Gustavo, B., Iryna, V., Clas, P., Hans, A., Gunnar, A. N., & Lars, Ö. (2013). Electronic and optical properties of nanocrystalline WO3 thin films studied by optical spectroscopy and density functional calculations. *Journal of Physics: Condensed Matter, 25*(20), 205502.
Mangalam, R. V. K., Ray, N., Waghmare, U. V., Sundaresan, A., & Rao, C. N. R. (2009). Multiferroic properties of nanocrystalline BaTiO3. *Solid State Communications, 149*(1–2), 1-5. doi: http://dx.doi.org/10.1016/j.ssc.2008.10.023
Manolis, A. (1983). The diagnostic potential of breath analysis. *Clin Chem, 29*(1), 5-15.
Marco, R., & Antonio, T. (2011). Toward portable breath acetone analysis for diabetes detection. *Journal of Breath Research, 5*(3), 037109.
Matthias, B. T. (1949). Ferro-electric Properties of WO3. *Physical Review, 76*(3), 430-431.
Musil, J., & Kadlec, S. (1990). Reactive sputtering of TiN films at large substrate to target distances. *Vacuum, 40*(5), 435-444. doi: http://dx.doi.org/10.1016/0042-207X(90)90241-P
Okuyama, K., & Wuled Lenggoro, I. (2003). Preparation of nanoparticles via spray route. *Chemical Engineering Science, 58*(3–6), 537-547. doi: http://dx.doi.org/10.1016/S0009-2509(02)00578-X
Patil, P. S. (1999). Versatility of chemical spray pyrolysis technique. *Materials Chemistry and Physics, 59*(3), 185-198. doi: http://dx.doi.org/10.1016/S0254-0584(99)00049-8
Purwanto, A., Wang, W. N., & Okuyama, K. (2011). Flame Spray Pyrolysis. In N. Ashgriz (Ed.), *Handbook of Atomization and Sprays* (pp. 869-879): Springer US.
Safi, I. (2000). Recent aspects concerning DC reactive magnetron sputtering of thin films: a review. *Surface and Coatings Technology, 127*(2–3), 203-218. doi: http://dx.doi.org/10.1016/S0257-8972(00)00566-1
Salje, E., & Viswanathan, K. (1975). Physical-Properties and Phase-Transitions in WO3. *Acta Crystallographica Section A, A 31*(May1), 356-359. doi: Doi 10.1107/S0567739475000745
Sawada, S. (1956). Thermal and Electrical Properties of Tungsten Oxide (WO3). *Journal of the Physical Society of Japan, 11*(12), 1237-1246. doi: 10.1143/JPSJ.11.1237
Schick, J. T., Jiang, L., Saldana-Greco, D., & Rappe, A. M. (2014). Coupling between octahedral rotations and local polar displacements in WO3/ReO3 superlattices. *Physical Review B, 89*(19), 195304.
Sigmund, P. (1981). Sputtering by ion bombardment theoretical concepts. In R. Behrisch (Ed.), *Sputtering by Particle Bombardment I* (Vol. 47, pp. 9-71): Springer Berlin Heidelberg.
Souza-Filho, A. G., Freire, V. N., Sasaki, J. M., Mendes Filho, J., Julião, J. F., & Gomes, U. U. (2000). Coexistence of triclinic and monoclinic phases in WO3 ceramics. *Journal of Raman Spectroscopy, 31*(6), 451-454. doi: 10.1002/1097-4555(200006)31:6<451::AID-JRS528>3.0.CO;2-K

Souza Filho, A. G., Freire, P. T. C., Pilla, O., Ayala, A. P., Mendes Filho, J., Melo, F. E. A., . . . Lemos, V. (2000). Pressure effects in the Raman spectrum of WO3 microcrystals. *Physical Review B, 62*(6), 3699-3703.

Strobel, R., & Pratsinis, S. E. (2007). Flame aerosol synthesis of smart nanostructured materials. *Journal of Materials Chemistry, 17*(45), 4743-4756. doi: 10.1039/B711652G

Suvarna, R. B., & Patil, P. S. (2007). Influence of Nb doping on the electrochromic properties of WO3 films. *Journal of Physics D: Applied Physics, 40*(23), 7423.

Swihart, M. T. (2003). Vapor-phase synthesis of nanoparticles. *Current Opinion in Colloid & Interface Science, 8*(1), 127-133. doi: http://dx.doi.org/10.1016/S1359-0294(03)00007-4

Tanisaki, S. (1960a). Crystal Structure of Monoclinic Tungsten Trioxide at Room Temperature. *Journal of the Physical Society of Japan, 15*(4), 573-581. doi: Doi 10.1143/Jpsj.15.573

Tanisaki, S. (1960b). On the Phase Transition of Tungsten Trioxide Below Room Temperature. *Journal of the Physical Society of Japan, 15*(4), 566-573. doi: Doi 10.1143/Jpsj.15.566

Tassopoulos, C. N., Barnett, D., & Russell Fraser, T. (1969). BREATH-ACETONE AND BLOOD-SUGAR MEASUREMENTS IN DIABETES. *The Lancet, 293*(7609), 1282-1286.

Teoh, W. Y., Amal, R., & Madler, L. (2010). Flame spray pyrolysis: An enabling technology for nanoparticles design and fabrication. *Nanoscale, 2*(8), 1324-1347. doi: 10.1039/C0NR00017E

Tilley, R. J. D. (1995). The crystal chemistry of the higher tungsten oxides. *International Journal of Refractory Metals and Hard Materials, 13*(1–3), 93-109. doi: http://dx.doi.org/10.1016/0263-4368(95)00004-6

Vladimir, M. F. (2006). Critical size in ferroelectric nanostructures. *Physics-Uspekhi, 49*(2), 193.

Wang, F., Di Valentin, C., & Pacchioni, G. (2011). Electronic and Structural Properties of WO3: A Systematic Hybrid DFT Study. *The Journal of Physical Chemistry C, 115*(16), 8345-8353. doi: 10.1021/jp201057m

Wang, L., Teleki, A., Pratsinis, S. E., & Gouma, P. I. (2008). Ferroelectric WO3 Nanoparticles for Acetone Selective Detection. *Chemistry of Materials, 20*(15), 4794-4796. doi: 10.1021/cm800761e

Woodward, P. M., Sleight, A. W., & Vogt, T. (1997). Ferroelectric Tungsten Trioxide. *Journal of Solid State Chemistry, 131*(1), 9-17. doi: http://dx.doi.org/10.1006/jssc.1997.7268

Xu, Y., Carlson, S., & Norrestam, R. (1997). Single Crystal Diffraction Studies of WO3 at High Pressures and the Structure of a High-Pressure WO3 Phase. *Journal of Solid State Chemistry, 132*(1), 123-130.

Yun, Y., & Altman, E. I. (2007). Using ferroelectric poling to change adsorption on oxide surfaces. *J Am Chem Soc, 129*(50), 15684-15689. doi: 10.1021/ja0762644

Zhang, X., Huo, K., Hu, L., & Chu, P. K. (2010). Fabrication and Photocatalytic Activity of Nanoporous WO₃ Film. *Nanoscience and Nanotechnology Letters, 2*(1), 51-57. doi: 10.1166/nnl.2010.1052

Zhao, H., Qu, Z.-R., Ye, H.-Y., & Xiong, R.-G. (2008). In situ hydrothermal synthesis of tetrazole coordination polymers with interesting physical properties. *Chemical Society Reviews, 37*(1), 84-100. doi: 10.1039/B616738C

Zheng, H., Ou, J. Z., Strano, M. S., Kaner, R. B., Mitchell, A., & Kalantar-zadeh, K. (2011). Nanostructured Tungsten Oxide – Properties, Synthesis, and Applications. *Advanced Functional Materials, 21*(12), 2175-2196. doi: 10.1002/adfm.201002477

Zhong, W., Wang, Y., Zhang, P., & Qu, B. (1994). Phenomenological study of the size effect on phase transitions in ferroelectric particles. *Physical Review B, 50*(2), 698-703.

Lisheng Wang, "Tailored Synthesis and Characterization of Selective Metabolite-detecting nanoprobes for Handheld Breath Analysis", Ph.D. thesis, SUNY Stony Brook, Dec 2008